Interference and SINR in Millimeter Wave and Terahertz Communication Systems With Blocking and Directional Antennas

Vitaly Petrov, *Student Member, IEEE*, Mikhail Komarov, *Member, IEEE*, Dmitri Moltchanov, Josep Miquel Jornet, *Member, IEEE*, and Yevgeni Koucheryavy, *Senior Member, IEEE*

***Abstract*— The fifth generation wireless systems are expected to rely on a large number of small cells to massively offload traffic from the cellular and even from the wireless local area networks. To enable this functionality, mm-wave (EHF) and Terahertz (THF) bands are being actively explored. These bands are characterized by unique propagation properties compared with microwave systems. As a result, the interference structure in these systems could be principally different to what we observed so far at lower frequencies. In this paper, using the tools of stochastic geometry, we study the systems operating in the EHF/THF bands by explicitly capturing three phenomena inherent for these frequencies: 1) high directivity of the transmit and receive antennas; 2) molecular absorption; and 3) blocking of high-frequency radiation. We also define and compare two different antenna radiation pattern models. The metrics of interest are the mean interference and the signal-to-interference-plus-noise (SINR) ratio at the receiver. Our results reveal that: 1) for the same total emitted energy by a Poisson field of interferers, both the interference and SINR significantly increase when simultaneously both transmit and receive antennas are directive and 2) blocking has a profound impact on the interference and SINR creating much more favorable conditions for communications compared with no blocking case.**

***Index Terms*— Interference, millimeter waves, terahertz band, directional antennas, blocking, 5G systems.**

I. Introduction

TO KEEP up with constantly increasing traffic demands and quality of service requirements [2], industry is preparing for a 1000x increase in mobile data [3]. Despite the significant steps forward, current 4G cellular technologies will soon be insufficient to satisfy the constantly growing device base and customer traffic demands.

Manuscript received June 2, 2016; revised October 21, 2016; accepted January 3, 2017. Date of publication January 17, 2017; date of current version March 8, 2017. This work was supported by the Academy of Finland FiDiPro Program Nanocommunication Networks 2012–2016. The work of J. M. Jornet was supported by AFRL under Grant FA8750-15-1-0050. The work of V. Petrov was supported by the Nokia Foundation. This paper was presented at the Proceedings of the IEEE Globecom'16 [1]. The associate editor coordinating the review of this paper and approving it for publication was A. Zajic.

V. Petrov, M. Komarov, D. Moltchanov, and Y. Koucheryavy are with the Department of Electronics and Communications Engineering, Tampere University of Technology, 33720 Tampere, Finland (e-mail: vitaly.petrov@tut.fi; dmitri.moltchanov@tut.fi; yk@cs.tut.fi).

J. M. Jornet is with the Department of Electrical Engineering, University at Buffalo, The State University of New York, New York, NY 14260 USA (e-mail: jmjornet@buffalo.edu).

Color versions of one or more of the figures in this paper are available online at http://ieeexplore.ieee.org.

Digital Object Identifier 10.1109/TWC.2017.2654351

Among the possible solutions, future generation of wireless systems are expected to rely on high-capacity small cells to offload heavy traffic from the cellular and even local area networks. To enable this, millimeter wave systems operating in the EHF band (30–300GHz) have been heavily investigated in the recent years [4]. Furthermore, several groups are already exploring the use of even higher frequency windows available in the Terahertz band (THF, 0.3–3THz), e.g., 300GHz, 640GHz, or even the entire THz window [5]–[10].

There are a number of critical factors that affect the propagation of waves in the EHF and THF bands, which will shape the interference in 5G systems. First of all, electromagnetic (EM) waves at these frequencies are affected by inherently very high pathloss [11] as the much smaller size of EHF/THF antennas results in a large spreading loss. Molecular absorption further hampers the signal propagation. This phenomenon reflects the process by which a part of the EM energy of the propagating signal is converted into kinetic energy in internally vibrating molecules. In the EHF band, oxygen, which is abundant in the atmosphere, affects the path loss [12]. For the THF band, water vapor serves the role of primary absorbent [13], [14]. Irrespective of the type of absorbent, the result is a more complex expression for the received power at a distance from the transmitter, which now includes not only the power law function but an exponent as well.

Given the transmission power constraints, highly directional antennas are needed at the transmitter (Tx) and/or receiver (Rx) to overcome the severe propagation losses. The belief is that high directivity of Tx/Rx antennas will eventually lead to a noise-limited regime of communications systems [15]. However, razor-sharp-beam interference-free communications are not on the immediate horizon. The reasons range from the complexity of high directivity beamforming antennas to the synchronization challenges that they introduce. In addition, it has been experimentally shown that interference may still play a substantial role in specific environments [4]. The increasing network densification [16], the use of advanced networking mechanisms such as pico/femto cells [17], client-relays [18], and direct device-to-device communications [19] may still cause interference even when directional antennas are used.

Another effect to take into account is line-of-sight (LoS) blockage. This phenomenon has been addressed in a number of papers in the context of microwave communication sys-

tems [20], [21], where buildings block the path between Tx and Rx. Millimeter-wave and THz systems are expected to operate over much shorter distances than microwave cellular systems and, thus, buildings are not expectedly a major problem in outdoor deployments [12]. However, at these frequencies, users themselves may block the LoS path between Tx and Rx, as almost any object whose volume is larger than several wavelengths (millimeters in in the bands of interest) is effectively an obstacle. Recent measurements and simulations report that up to 60∼80% of energy available at the Rx comes from the LoS component and dictates the channel quality [12], [22]–[24]. Therefore, the process of LoS possible blockage by users has also to be taken into account in performance modeling of EHF and THF communications systems.

Despite the many existing works in the broad field of multi-user interference modeling, which we summarize in Sec. II, to the best of our knowledge, there is no study that simultaneously captures all these effects. In this paper, using the tools of stochastic geometry, we develop an analytical model of interference and SINR for systems operating in the EHF and THF bands that explicitly captures the following three effects inherent for these frequencies: (i) directivity of the Tx and Rx antennas, (ii) additional path loss component caused by molecular absorption, and (iii) blocking of high frequency radiation. Two radiation pattern models of directional antennas are considered, namely, the *cone* model representing an ideal directional antenna, and the *cone-plus-sphere* model capturing specifics of a non-ideal directional antenna with side lobes. The metrics of interest are the mean interference and the SINR at the receiver.

Using the developed model, we numerically investigate the multi-user interference in different scenarios. Our results show that the mean interference increases when the Tx or the Rx or both are equipped with directional antennas. However, the associated increase in the useful signal strength effectively compensates this effect and the SINR drastically improves showing that EHF/THF communication systems can indeed be designed to be noise-limited in the most cases. The effect of blocking further improves the performance in terms of SINR while the molecular absorption substantially degrades it.

The rest of the paper is organized as follows. In Sec. II, we provide a brief account of previous studies on interference estimation for directional antennas and blocking. In Sec. III, we review the propagation characteristics of EHF and THF bands and introduce the antenna and network models for our study. The mathematical models of interference and mean value of SINR are derived in Sec. IV and Sec. V, respectively. Numerical results are reported and discussed in Sec. VI. The conclusions are drawn in Sec. VII.

II. Related Work

Many stochastic models of interference have been developed to date. An extensive review of the existing models can be found in [25]–[27]. Typically, these models assume a random isotropic and homogenous deployments in $\Re^2$, such as Poisson Point Process [20], [28] or, rarely, Mattern hardcore process [29]. In most studies, the antenna radiation pattern is assumed to be omnidirectional and the path loss is a power law function of the distance [30], even the exponent value may be different for different communication ranges [31].

The models reported in the literature do not simultaneously capture all the effects of the EHF/THF bands. Recently, the studies addressing interference modeling in presence of directional antennas [32], [33] and signal blockage by human bodies [34], [35] in EHF band started to appear. The propagation model used in [32]–[35] neglects the exponential attenuation term caused by molecular absorption loss, while the model in [35] also assumes interferers located on the fixed positions, which is not realistic for dynamic environments. The interference and SIR analysis in presence of the absorption losses has been provided in [36]. However, the presented model neglects the effects of blocking. The study in [37] relies on a simple model of absorption presuming a constant attenuation coefficient and also neglects the effect of blocking. In addition, several simulation-based studies estimating the interference in mm-wave systems have been recently presented [38], [39]. However, their applicability to the wide range of frequencies, nodes densities, and antenna radiation patterns, is limited.

In [40], a stochastic interference model for pulse-based THz communications was developed by taking into account the impact of molecular absorption. The work has targeted nanoscale communication networks and, thus, the impact of directivity or blockage was not captured. In [41], a model for continuous-wave THz communications was developed to compute also the SINR under similar assumptions. In both cases, the results show that for an omnidirectional antenna pattern the interference has similar structure to what is observed at lower frequencies. At the same time, specifics of THz waves propagation, namely, molecular absorption (see Section III-A) has a notable quantitive effect on the mean interference level and SINR values. Therefore, the effect of molecular absorption should not be avoided in interference modeling for more sophisticated scenarios.

The impact of multi-user interference at the link layer has been addressed in several recent studies. In [42], the authors study the collision probability in mm-wave networks. The analysis takes into account the antenna directivity and molecular absorption, but does not incorporate blockage and is performed exclusively for the selected channel access method. In [43], the authors develop a collision-aware scheduling scheme for mm-waves, ignoring the blockage and molecular absorption effects. There have been many other directional MAC protocols, including [44], [45] and our recent work in [46], but none of these works either estimate the interference level in a random deployment or incorporate other important propagation effects.

III. Propagation, Antenna Radiation Pattern, and Network Models

In this section, we introduce the system model. Our notation is summarized in Table I.

A. Propagation in EHF/THF Bands

The distinguishing feature of the EHF/THF channels is the presence of molecular absorption [13], [47], albeit much

TABLE I
NOTATION USED IN THE PAPER

Parameter	Definition
System parameters	
P_{Tx_0}	Emitted power at the tagged transmitter
P_{Rx_0}	Received power at the tagged receiver
r_0	The distance between Rx_0 and Tx_0
r_i	The distances between interferers/blockers and Rx_0
r_B	Radius of interferer/blocker
$r^\star$	Radius for side lobe approximation
R	The interference zone around the tagged receiver
λ_I	The intersity of interferers/blockers in the area
Propagation model parameters	
K	Absorption coefficient, $K \in (0,1)$
$S_{Rx}(f,r)$	Received signal psd
$L_P(f,r)$	Propagation losses
$L_A(f,r)$	Absorption losses
$S_M(f,r)$	Molecular noise psd
$S_{JN}(f)$	Johnson-Nyquist thermal noise psd
$S_T(f,r)$	Total noise psd
k_B	Boltzmann constant
T	Temperature in Kelvin
h	Plank constant
$\tau(f,r)$	Transmittance of the medium
f	Operational frequency
Antenna model parameters	
G, G_1, G_2	Antenna gains
k	Coefficient of losses to the side lobes, $k \in (0,1)$
α	Antenna directivity angle
H	Tx power + frequency-dependant loss coefficient (introduced in (15) to simplify derivations)
A, A_1, A_2	Tx power + frequency-dependant loss + gains coefficient (introduced in (15) to simplify derivations)
Blocking model parameters	
l_A	Length of an arc of the circumference
λ_P	Intensity of projections of blockers
L	Distance from the receiver to a blocker
W	Blocked interval created by a single blocker
v_i	Renewal points associated with blocking process
V	Length of a single blocked/unblocked interval
$p_B(x), p_A(x)$	Probability that a random point in blocked/unblocked
Interference and SINR models parameters	
I	Aggregate interference
$Ei(\cdot)$	Exponential integral function
$E[\cdot]$	Mean value
S	Signal-to-interference-plus-noise ratio
p_C	Probability that interferer affects Rx_0
Λ	Intensity of the unblocked interferers
$r_\star$	Radius of side lobe's effect
N	Number of interferers in the circle of radius R
N_O	The mean number of interferers affecting Rx_0
$W(\cdot)$	Lambert W function
$\Gamma(\cdot,\cdot)$	The incomplete Gamma function
C	Normalization constant
G	Interference from a single node
λ_E	Intensity of the thinned process

stronger in the THF band. In the former, especially, in the unlicensed 60GHz band, absorption is dominated by O_2 molecules; in the latter, absorption is mainly caused by H_2O vapor [14]. These losses make the wireless channel highly frequency selective. The received power spectral density (psd) in the EHF/THF band can written as

$$S_{Rx}(f,r) = \frac{S_{Tx}(f) G_{Tx}(f)\, G_{Rx}(f)}{L_A(f,r) L_P(f,r)}, \tag{1}$$

where f is the operating frequency, r is the separation distance between the transmitter and the receiver, $S_{Tx}(f)$ stands for the transmitted signal psd, $L_A(f,r)$ represents the absorption loss, $L_P(f,r)$ is the spreading loss, and $G_{Tx}(f)$ and $G_{Rx}(f)$ refer to the antenna gains in transmission and reception, respectively, which we consider to be constant within the specific transmission window (and, thus, we remove their dependence on f from now on).

Following [13], the absorption loss is defined as

$$L_A(f,r) = \frac{1}{\tau(f,r)}, \tag{2}$$

where $\tau(f,r)$ is the transmittance of the medium following the Beer-Lambert law, $\tau(f,r) \approx e^{-K(f)r}$, $K(f)$ is the overall absorption coefficient of the medium available from the HITRAN database [14]. The propagation loss is obtained under the assumption of spherical propagation in free space, i.e., $L_P(f,r) = (4\pi r f/c)^2$, where c refers to the speed of the EM wave.

In addition to the path loss, we have to specify the noise in THz band. First, the EM radiation absorbed by the molecules in the medium is re-radiated out-of-phase at approximately the same frequencies it has been absorbed. This is known as the medium emissivity [48] and, from the communication perspective, it is considered as a noise source [13]. Following [13], [49], the molecular absorption noise psd is

$$S_M(f,r) = \frac{S_{Tx}(f) G_{Tx} G_{Rx}}{L_P(f,r)} [1 - \tau(f,r)]. \tag{3}$$

As of now, there is still no definite conclusion whether this noise is high enough to affect the reception (we refer the readers to [50] for detailed discussion on molecular noise). However, as we will see in what follows, the presence/absence of this noise affects SINR analysis. In this paper we address both cases.

The second contributor to the noise is the Johnson-Nyquist noise generated by thermal agitation of electrons in conductors. The form of this noise changes when entering the EHF/THF frequencies. Its power stays flat up until 0.1THz at $P_{JN} = k_B T = -174$dBm/Hz, where k_B is the Boltzmann constant and T is the temperature in Kelvin, and then it declines non-linearly up until approximately 6THz [51]. Thus, the Johnson-Nyquist noise is a function of the operating frequency and we approximate its psd using [51]

$$S_{JN}(f) = \frac{hf}{\exp(hf/k_B T) - 1}, \tag{4}$$

where h is Planck's constant.

Summarizing, the total noise psd at the receiver is

$$S_T(f,d) = \frac{hf}{\exp(hf/k_B T) - 1} + \frac{S_{Tx}(f) G_{Tx} G_{Rx} [1 - \tau(f,r)]}{L_P(f,r)}. \tag{5}$$

B. Antenna Radiation Pattern Models

We consider two antenna radiation pattern models (see Fig. 1), namely, the cone model and the cone-plus-sphere model. In the first model, Fig. 1(a), the antenna radiation pattern is modeled with a single cone-shaped beam, whose width determines the antenna directivity. The second model, Fig. 1(b), takes into account the presence of side-lobes around the single main lobe, which are modeled as a sphere around

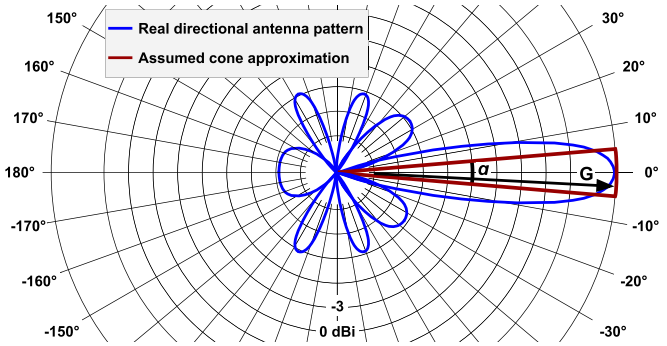

(a) Cone

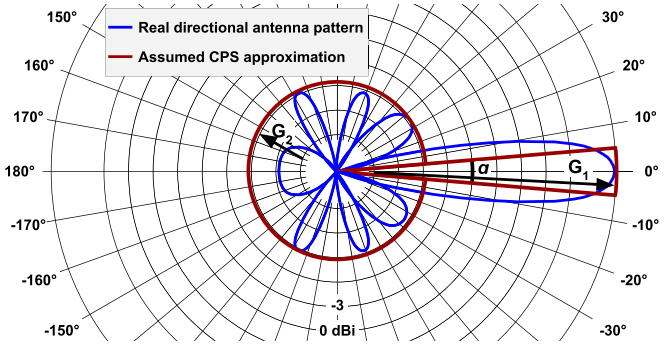

(b) Cone-Plus-Sphere (CPS)

Fig. 1. Illustration of the considered antenna radiation pattern models.

the antenna. Whereas the first antenna radiation diagram corresponds to a rather ideal directional antenna, the second model can be understood as a simplified model for a more realistic antenna.

To parameterize the cone model, we need to provide the antenna gain G for the single lobe with directivity angle α. For the second model, G_1 and G_2, corresponding to the gains for the main and side lobes, respectively, have to be provided. The gains G, G_1, and G_2 will be used to amplify the signal with respect to the direction it goes to or comes from.

1) Cone Model: For this antenna radiation pattern, the psd $\mathcal{P}_{Rx}$ at a distance r is

$$\mathcal{P}_{rx} = \frac{P_{Tx}}{S_A} = \frac{P_{Tx}}{2\pi r h}, \tag{6}$$

where S_A is the surface area of the wavefront, given by the surface area of the spherical cap, with $h = r[1 - \cos(\alpha/2)]$, and α is the antenna directivity angle.

Alternatively, according to free-space propagation model, the psd $\mathcal{P}_{Rx}$ at the wavefront is

$$\mathcal{P}_{Rx} = \frac{P_{Tx}}{S_A} = P_{Tx}\frac{G}{4\pi r^2}, \tag{7}$$

which implies that the antenna gain G for the main lobe in the cone model is given by

$$G = \frac{2}{1 - \cos(\alpha/2)}. \tag{8}$$

Note that for $\alpha = 2\pi$, i.e., an ideal omnidirectional antenna, the gain $G = 1$ and $S_A = 4\pi r^2$ as in omnidirectional spherical spreading.

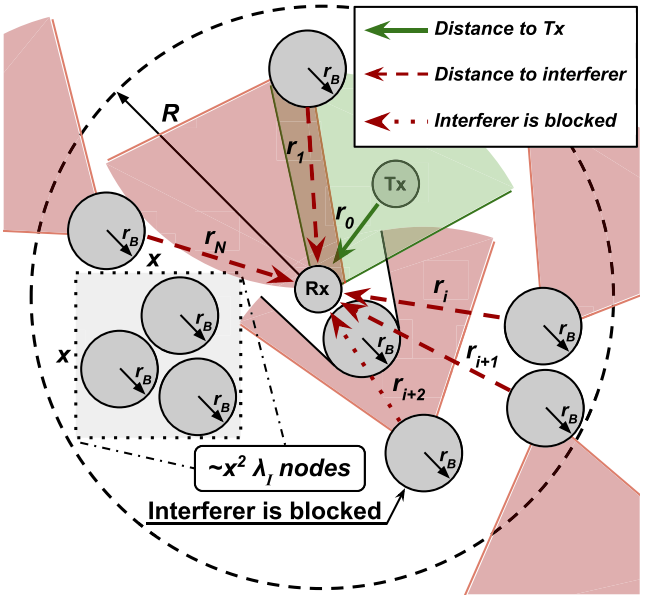

Fig. 2. An illustration of the considered network deployment.

2) Cone-Plus-Sphere Model: To parameterize this model we need to provide G_1 and G_2. Denoting the fraction of energy concentrated along the main lobe by k_1 and the one lost to side lobes by k_2, and following the same reasoning as for the cone model, we get the set of equations

$$\begin{cases} \mathcal{P}_{Rx1} 2\pi r^2[1 - \cos(\alpha/2)] = k_1 P_{Tx} \\ \mathcal{P}_{Rx2} 2\pi r^2[1 + \cos(\alpha/2)] = k_2 P_{Tx} \\ k_1 + k_2 = 1, \end{cases} \tag{9}$$

where, according to the free space propagation model,

$$\begin{cases} \mathcal{P}_{Rx1} = G_1 P_{Tx}/4\pi r^2 \\ \mathcal{P}_{Rx2} = G_2 P_{Tx}/4\pi r^2. \end{cases} \tag{10}$$

Thus, we have the following relation between G_1 and G_2

$$G_1[1 - \cos(\alpha/2)] + G_2[1 + \cos(\alpha/2)] = 2. \tag{11}$$

There are multiple solutions for (G_1, G_2). Setting $G_2 = 0$ reduces the model to cone antenna. Introducing $k = k_1/k_2$, $k \in (0, 1)$ we see that $G_2 = kG_1$ and G_1, G_2 are given by

$$\begin{cases} G_1 = 2[(1 - \cos(\alpha/2)) + k(1 + \cos(\alpha/2))]^{-1} \\ G_2 = kG_1. \end{cases} \tag{12}$$

We now have the relations to specify G, G_1, and G_2 as functions of α and k in such a way that total transmit power does not change with the antenna directivity. This allows us to further compare the interference levels in fair conditions.

C. Network Model

As the major emphasis of this study is to assess the interference and SINR in the EHF/THF bands communications, we consider a random nodes deployment in $\Re^2$, see Fig. 2. We model the field of interferers by a Poisson point process with intensity λ_I. We tag an arbitrary one and assign it as a Rx of interest, Rx_0. The associated Tx, denoted as Tx_0, is

chosen to be at the distance r_0 from the Rx_0. The rest of the nodes are considered as interferers. To model the respective receivers we assume that the orientation of the bisects of all coverage zones of transmitters are uniformly distributed in $(0, 2\pi)$. The radius of the zone where the nodes provide non-negligible interferences, R, can be computed using the propagation model. The transmissions of the nodes that are further than R is considered as noise. In our study, we consider interferers acting as blockers as well, i.e., a certain interferer residing along the path between another interferer and Rx_0 blocks the LoS path. Thus, depending on the context, the terms blocker and interferer are used interchangeably. The blockers are assumed to be of circular shape with radius r_B, see Fig. 2. The considered scenario corresponds to the case on "uncontrolled" direct communications in a random deployment providing the upper bound on the interference experienced by nodes.

D. Metrics of Interest

For the described scenario, the SINR is given by

$$S(\vec{r}, \vec{P}_T, f) = \frac{P_{Rx_0}(r_0, P_{Tx_0}, f)}{I(\vec{P}_{Tx}, \vec{r}, f) + S_N(\vec{P}_T, \vec{r}, f)}, \tag{13}$$

where $P_{Rx_0}(r_0, P_{Tx_0}, f)$ is the received signal power at a distance r_0, $I(\vec{P}_{Tx}, \vec{r}, f)$ is the aggregate power of the interferers at Rx_0, $S_N(\vec{P}_{Tx}, \vec{r}, f)$ is the total noise at Rx_0, $\vec{r}$ is the vector of distances between interferers and Rx_0, f is the frequency and N is the number of interfering nodes in the area of radius R. In this study, we consider no power control and assign $P_{Tx_i} = P_{Tx_j} = P_{Tx_0}$, $i, j = 0, 1, \ldots, N$. In what follows, for SINR, interference and noise we drop arguments that are often silently assumed, i.e., f, P_{Tx} and r_i.

The useful received power is given by

$$P_{Rx_0} = A r_0^{-2} e^{-K r_0}, \tag{14}$$

where we abstract the effect of transmission power, antenna gains, and path loss as

$$A = P_{Tx} G_{Tx} G_{Rx} \frac{c^2}{16\pi^2 f^2} = H G_{Tx} G_{Rx}, \tag{15}$$

where $H = P_{Tx} c^2/(16\pi^2 f^2)$ to simplify further derivations. The values for antenna gains at Tx and Rx sides, G_{Tx} and G_{Rx}, can be obtained as described in Section III-B.

The aggregate interference is then

$$I = A \sum_{i=1}^{N} r_i^{-2} e^{-K r_i}. \tag{16}$$

where N is a random variable (RV) denoting the number of interferers and, for clarity, the cone radiation pattern is assumed (we provide elaborated equations for the cone-plus-sphere antenna radiation pattern in the following section).

The expression in the denominator of SINR depends on whether we take into account the effect of molecular noise or not. When molecular noise is present, the aggregated noise is written as

$$S_N = S_{JN} + A \sum_{i=0}^{N} r_i^{-2} (1 - e^{-K r_i}). \tag{17}$$

Since $A r_i^{-2}(1 - e^{-K r_i}) + A r_i^{-2} e^{-K r_i} = A r_i^{-2}$, the denominator of (13) can be written as

$$S_{JN} + I = S_{JN} + A \sum_{i=1}^{N} r_i^{-2}. \tag{18}$$

Substituting (17) and (18) into (13) gives the following expression for the SINR

$$S = \frac{A r_0^{-2} e^{-K r_0}}{S_{JN} + A \sum_{i=1}^{N} r_i^{-2}}. \tag{19}$$

The expression (19) is a generic one with all the phenomena taken into account. Depending on 1) the type of technology used for receiver design, 2) the frequency band and 3) the assumption about the molecular noise, we can distinguish between a number of special cases. For conventional transceiver technology such as silicon germanium and frequencies below 6THz there is always the thermal noise introduced by the receiver S_{JN}. If the principal parts of the transceivers are made of superconductive materials, such as graphene, and/or the frequency of interest is higher than 6THz the thermal noise is negligible [51], [52].

When molecular noise is ignored, (19) reduces to

$$S = \frac{A r_0^{-2} e^{-K r_0}}{S_{JN} + A \sum_{i=1}^{N} r_i^{-2} e^{-K r_i}}. \tag{20}$$

Below, we first characterize interference according to (20) assuming that the effect of molecular noise is negligible. We then extend the analysis to the case of molecular noise. In Sec. V we characterize mean SINR for both (19) and (20).

IV. Characterization of Mean Interference

A. Blocking Model

In a Poisson field of interferers, the nodes themselves act as blockers for interference LoS paths. We assume that if the interference LoS path between a certain interferer and the Rx_0 is blocked by another interferer, the interference at the Rx_0 is zero. Let us fix a distance from the interferer to Rx_0, x. In Appendix A, we show that the blocking probability is given by

$$p_B(x) = 1 - e^{-\lambda_I (x - r_B) r_B}, \tag{21}$$

where r_B is the blocker radius.

Note that in addition to interferers, other humans currently not participating in the communications may also block the interference LoS paths. Modeling this process as an Poisson process with intensity λ_B we can still apply (21) with intensity $(\lambda_I + \lambda_B)$.

Using (21), the blocking probability as a function of the distance, x, for different values of λ_I and r_B is plotted in Fig. 3. As one may observe, the blocking probability tends to one exponentially fast when $x \to \infty$. Also, the higher the intensity λ_I, the higher the blocking probability. The radius of blockers, r_B, also affects the value of p_B. Expectedly, for larger radii the blocking probability is higher.

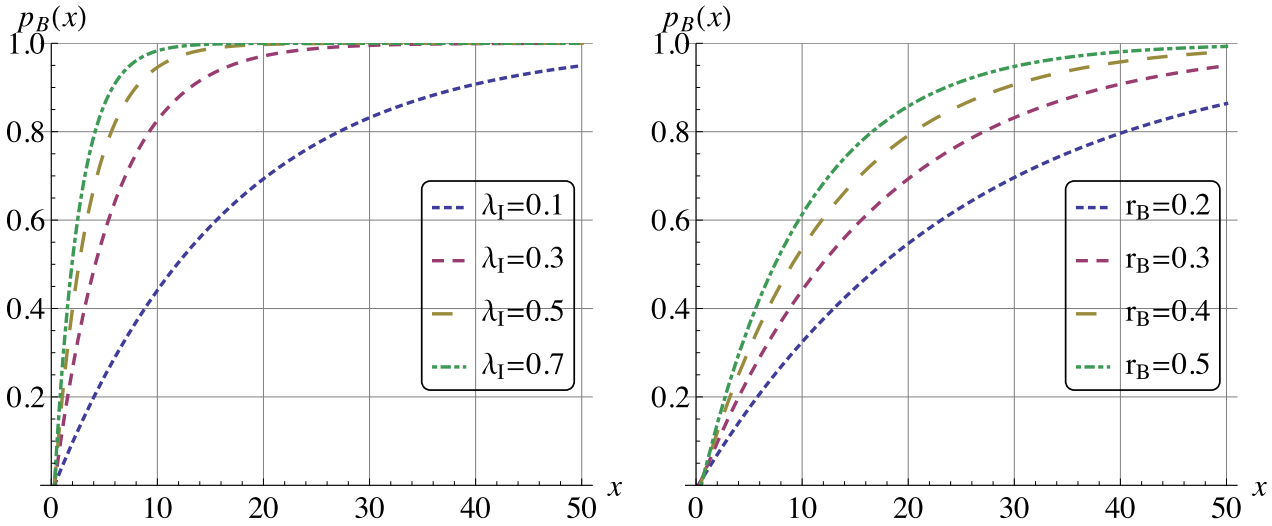

(a) Different λ_I (b) Different r_B

Fig. 3. Probability of blocking as a function of the separation distance x.

B. Cone Antenna Model

Consider the case of directional antenna at either Tx or Rx first. There are two cases when an interferer located at distance x does not contribute to the interference at the Rx_0: (i) its contribution is blocked by other interferers, and (ii) the Rx_0 is not in coverage of the interferer. The former happens with probability p_B, derived previously. The probability that Rx_0 is not in coverage of the interferer is independent of the distance x and given by

$$p_C = \frac{\alpha x}{2\pi x} = \frac{\alpha}{2\pi}. \tag{22}$$

Consider the infinitesimal radial increment dr. Since the process of blockers/interferers is Poisson, multiple events are not allowed to happen within dr and the probability that the interferer is located at distance r is proportional to the increment of the area dr. The area increment is

$$\pi(r+dr)^2 - \pi r^2 = 2\pi r dr + O(1), \tag{23}$$

implying that the probability that interferer is in $(r, r+dr)$ is $2\lambda_I \pi r dr$.

When the interferer located at the distance r is not blocked and the Rx_0 is in its coverage area, the contribution to the interference is $Ar^{-2}e^{-Kr}$. Thus, the mean interference is

$$E[I] = \int_{r_B}^{R} Ar^{-2}e^{-Kr} p_C[1 - p_B(r)]2\lambda_I \pi r dr. \tag{24}$$

Substituting (21) and (22) into (24) we get

$$\begin{aligned} E[I] &= \int_{r_B}^{R} Ar^{-2}e^{-Kr} e^{-\lambda_I (x-r_B) r_B} \frac{\alpha}{2\pi} 2\lambda_I \pi r dr \\ &= A\alpha\lambda_I \Theta(R, r_B, \lambda_I, K), \end{aligned} \tag{25}$$

where $\Theta(R, r_B, \lambda_I, K)$ is given by

$$\begin{aligned} \Theta = {} & e^{-\lambda_I r_B^2} Ei(-R[K + \lambda_I r_B]) \\ & - Ei(-r_B^2[K + r_B \lambda_I]), \end{aligned} \tag{26}$$

and $Ei(\cdot)$ is the exponential integral function.

When blocking is not taken into account, we get

$$E[I] = A\alpha\lambda_I \int_{r_B}^{R} \frac{1}{r} e^{-Kr} dr = A\alpha\lambda_I \Theta_1(R, r_B, K), \tag{27}$$

where $\Theta_1(R, r_B, K) = Ei(-KR) - Ei(-Kr_B)$.

When the antenna is omnidirectional, we arrive at

$$E[I] = 2\pi\lambda_I A \Theta(R, r_B, \lambda_I, K), \tag{28}$$

Similarly, for omnidirectional antennas and no blocking we have

$$E[I] = 2\pi\lambda_I A \Theta_1(R, r_B, K). \tag{29}$$

Finally, when directivity at both sides is assumed we have

$$\begin{aligned} \text{Blocking: } E[I] &= \frac{A\alpha^2\lambda_I}{2\pi} \Theta(R, r_B, \lambda_I, K), \\ \text{No blocking: } E[I] &= \frac{A\alpha^2\lambda_I}{2\pi} \Theta_1(R, r_B, \lambda_I, K). \end{aligned} \tag{30}$$

C. Cone-Plus-Sphere Antenna Model

For the cone-plus-sphere antenna, we have to distinguish between three cases for an individual interferer: (i) interferer's LoS path is blocked, (ii) interferer's LoS path is not blocked and points to the Rx_0 with its main lobe, and (iii) interferer's LoS path is not blocked and points to the Rx_0 with its side/back lobes. The probability of the first event is p_B and the contribution of the interferer to the total interference is 0. The probability of the second event is $p_c(1 - p_B)$ and the contribution can be expressed via (25) with A_1 gain replacing A. The third event happens with the probability $(1 - p_c)(1 - p_B)$ and the contribution can be estimated by extending the result from (25) with A_2 replacing A. The mean interference for cone-plus-sphere antenna model is

$$\begin{aligned} E[I] = {} & \int_{r_B}^{R} A_1 r^{-2} e^{-Kr} p_C p_A 2\lambda_I \pi r dr \\ & + \int_{r_B}^{R} A_2 r^{-2} e^{-Kr} (1 - p_C) p_A 2\lambda_I \pi r dr. \end{aligned} \tag{31}$$

Evaluating the integrals in (31) we arrive at

$$E[I] = A_1\alpha\lambda_I\Theta(R, r_B, \lambda_I, K) + A_2[2\pi - \alpha]\lambda_I\Theta(R, r_B, \lambda_I, K). \quad (32)$$

When blocking is not taken into account we have

$$E[I] = A_1\alpha\lambda_I\Theta_1(R, r_B, K) + A_2[2\pi - \alpha]\lambda_I\Theta_1(R, r_B, K). \quad (33)$$

For directive antennas at both Tx and Rx, we obtain

$$\text{Blocking:} \quad E[I] = \frac{A_1\alpha^2\lambda_I}{2\pi}\Theta(R, r_B, \lambda_I, K) + \frac{A_2[2\pi - \alpha^2]\lambda_I}{2\pi}\Theta(R, r_B, \lambda_I, K),$$

$$\text{No blocking:} \quad E[I] = \frac{A_1\alpha^2\lambda_I}{2\pi}\Theta_1(R, r_B, K) + \frac{A_2[2\pi - \alpha^2]\lambda_I}{2\pi}\Theta_1(R, r_B, K). \quad (34)$$

Note that different directivity at Rx and Tx can also be modeled.

D. Interference in Presence of Molecular Noise

When molecular noise is taken into account, the mean interference for the cone model is

$$E[I] = \int_{r_B}^{R} Ar^{-2}e^{-\lambda_I(x-r_B)r_B}\frac{\alpha}{2\pi}2\lambda_I\pi r dr = A\alpha\lambda_I\Theta_1^{\star}(R, r_B, \lambda_I), \quad (35)$$

where the term $\Theta_1^{\star}(R, r_B, \lambda_I)$ is

$$\Theta_1^{\star}(R, r_B, \lambda_I) = e^{-\lambda_I r_B}E(-\lambda_I r_B R) - E(-\lambda_I r_B^2). \quad (36)$$

The difference compared to the absence of molecular noise is that the interfering power at the receiver from a single node is now Ar^{-2} instead of $Ar^{-2}e^{-Kr}$ due to additional contribution of molecular noise, $Ar_0^{-2}(1 - e^{-Kr_0})$.

Similarly, for cone-plus-sphere model we have

$$E[I] = A_1\alpha\lambda_I\Theta_1^{\star}(R, r_B, \lambda_I) + A_2[2\pi - \alpha]\lambda_I\Theta_1^{\star}(R, r_B, \lambda_I). \quad (37)$$

For directive antennas at both Tx and Rx we have

$$\text{Cone:} \quad E[I] = \frac{A\alpha^2\lambda_I}{2\pi}\Theta_1^{\star}(R, r_B, \lambda_I)$$

$$\text{CPS:} \quad E[I] = \frac{A_1\alpha^2\lambda_I}{2\pi}\Theta_1^{\star}(R, r_B, \lambda_I, K) + \frac{A_2[2\pi - \alpha^2]\lambda_I}{2\pi}\Theta_1^{\star}(R, r_B, \lambda_I, K). \quad (38)$$

V. SIR AND SINR FUNCTIONS

As discussed in Sec. III, SIR and SINR are the functions of the interference. According to the conventional approach, to determine these metrics one has to first obtain the distribution of interference and then transform this distribution to the metrics of interest. The distribution of interference is obtained by finding the distribution of each component $Ar_i^{-2}e^{-Kr_i}$ and then either switching to the transform domain to obtain the sum of RVs $\sum_{i=1}^{N} Ar_i^{-2}e^{-Kr_i}$, where N is a RV denoting the number of non-blocked interferers and r is the distance from the Rx_0 to an interfer or by directly approximating it with a certain distribution [41], [53].

Working with EHF/THF propagation with blocking effect, we face fundamental difficulties applying the abovementioned approach. First of all, the density of interferers is non-uniform over the circle as the blocking probability $p_B(x)$ depends on the distance to the potential interferer. Secondly, switching to the transform domain is infeasible for the propagation model in hand as there is no closed form for Laplace transform of the interference from a single node, $Ae^{-Kr}r^{-2}$. On top of this, even if it would have been feasible (e.g., in case of power-law propagation and no blocking), the inversion of the resulting transform back to the RV domain is also infeasible in most cases implyingsg that we are limited to first few moments of the metric of interest.

To obtain approximations for the mean and variance of SIR and SINR functions we propose to use the Taylor expansion technique outlined in Appendix B. Particularly, for the mean value of a RV $Y = g(X)$, where X is a RV with mean and variance μ_0 and $\sigma^2[X]$ we have

$$E[Y] = g(\mu_0) + \frac{g''(\mu_0)}{2}\sigma^2[X], \quad (39)$$

while for variance of $Y = g(X)$ we have

$$\sigma^2[Y] = [g'(\mu_0)]^2\sigma^2[X] - \frac{1}{4}[f''(\mu_0)\sigma^2[X]]^2. \quad (40)$$

The SIR and SINR functions are given by

$$g_1(x) = \frac{C}{x}, \quad g_2(x) = \frac{C}{S_{JN} + x}, \quad (41)$$

where $C = Ar_0^{-2}e^{-Kr_0}$, S_{JN} is the Johnson-Nyquist noise.

The first and second derivatives of (41) are

$$g_1'(x) = -\frac{C}{x^2}, \quad g_2'(x) = -\frac{C}{(S_{JN} + x)^2}, \quad g_1''(x) = \frac{2C}{x^3} \quad g_2''(x) = \frac{2C}{(S_{JN} + x)^3}. \quad (42)$$

The mean interference has been found in the previous section. To find mean and variance of the metrics of interest we need variance of interference provided in Appendix C. Now, for the mean SINR for directive antennas at one side only we arrive at (43), as shown at the top of next page, for blocking and no blocking cases, respectively, where r_0 is the separation distance between Tx and Rx, the functions $\Phi(R, r_B, \lambda_I, K)$ and $\Phi_1(R, r_B, K)$ are defined in Appendix C.

For the mean SINR for directive antennas at both Tx and Rx we have (44), as shown at the top of next page, for blocking and no blocking cases, respectively, where the functions $\Phi(R, r_B, \lambda_I, K)$ and $\Phi_1(R, r_B, K)$ are defined in Appendix C. The mean SINR in presence of molecular noise as well as the mean SIR for all considered cases can be obtained similarly. Note that getting higher moments of interference, e.g., skewness, excess, allows to increase the accuracy of approximations in (62), (66).

$$\text{Directional Tx or Rx} \begin{cases} \text{Blocking: } E[S] = \dfrac{Ae^{-Kr_0}r_0^{-2}}{S_{JN} + A\alpha\lambda_I\Theta(R, r_B, \lambda_I, K)} \\ \qquad + \dfrac{A^3e^{-Kr_0}r_0^{-2}[\alpha\lambda_I\Phi(R, r_B, \lambda_I, K) - [\alpha\lambda_I\Theta(R, r_B, \lambda_I, K)]^2]}{[S_{JN} + A\alpha\lambda_I\Theta(R, r_B, \lambda_I, K)]^3}, \\ \text{No blocking: } E[S] = \dfrac{Ae^{-Kr_0}r_0^{-2}}{S_{JN} + A\alpha\lambda_I\Theta_1(R, r_B, K)} \\ \qquad + \dfrac{A^3e^{-Kr_0}r_0^{-2}[\alpha\lambda_I\Phi_1(R, r_B, K) - [\alpha\lambda_I\Theta_1(R, r_B, K)]^2]}{[S_{JN} + A\alpha\lambda_I\Theta_1(R, r_B, K)]^3}, \end{cases} \tag{43}$$

$$\text{Directional Tx and Rx} \begin{cases} \text{Blocking: } E[S] = \dfrac{Ae^{-Kr_0}r_0^{-2}}{S_{JN} + \frac{A\alpha^2\lambda_I}{2\pi}\Theta(R, r_B, \lambda_I, K)} \\ \qquad + \dfrac{A^3e^{-Kr_0}r_0^{-2}[\frac{\alpha\lambda_I}{2\pi}\Phi(R, r_B, \lambda_I, K) - [\frac{\alpha^2\lambda_I}{2\pi}\Theta(R, r_B, \lambda_I, K)]^2]}{[S_{JN} + \frac{A\alpha^2\lambda_I}{2\pi}\Theta(R, r_B, \lambda_I, K)]^3}, \\ \text{No blocking: } E[S] = \dfrac{Ae^{-Kr_0}r_0^{-2}}{S_{JN} + \frac{A\alpha^2\lambda_I}{2\pi}\Theta_1(R, r_B, \lambda_I, K)} \\ \qquad + \dfrac{A^3e^{-Kr_0}r_0^{-2}[\frac{\alpha\lambda_I}{2\pi}\Phi_1(R, r_B, K) - [\frac{\alpha^2\lambda_I}{2\pi}\Theta_1(R, r_B, \lambda_I, K)]^2]}{[S_{JN} + \frac{A\alpha^2\lambda_I}{2\pi}\Theta_1(R, r_B, \lambda_I, K)]^3}, \end{cases} \tag{44}$$

VI. Numerical Results

In this section, we assess the effects of the radiation pattern model, antenna directivity, blocking, absorption loss and molecular noise on the mean interference and the mean SINR. For comparison purposes, throughout this section, we present the results assuming that interference coming from the nodes more than R from the receiver is zero, while the coefficient A, introduced in (15), equals to 1 for omnidirectional antenna ($H = 1$). The results for other models are relative to the omnidirectional one. In addition to A, (15) includes the frequency-dependent component of the path loss, related to the Rx antenna aperture. In the rest of this section, to qualitatively illustrate the dependencies of the metrics of interest on the continuum of values of the absorption coefficient K without referring to particular frequencies, we assume that this component is constant. Also, throughout this section the radius of the interference zone, R, around Rx_0 is set to 10.

A. Interference Assessment

1) The Effect of Directivity: In the first two subfigures in Fig. 4 the mean interference for scenarios with omni- and directional antennas is illustrated and compared to the simulation data when blocking is not taken into account. The *same emitted power* at all the nodes was assumed, absorption coefficient was set to $K = 0.01$ and blocking was not taken into account.

The simulation results have been obtained using an in-house-made simulator emulating the deployment scenarios. Simulated data points are indicated with markers of the same color in Fig. 4. As one may notice observing illustrations in Fig. 4, the analytical data closely resemble those of simulations confirming the accuracy of the proposed analysis. For this reason, in what follows, we illustrate the mean interference using analytical results only.

Analyzing Fig. 4(a) computed using (27), (29) and (30), we first note that all the models converge to the same value for $\alpha = 2\pi$ confirming our derivations. We see that using a directional antenna at Tx (or Rx) only results in much larger interference compared to omnidirectional case in the interval of most interest $(0, \pi)$. This is due to the fact that for small values of α both cone and cone-plus-sphere antenna radiation patterns concentrate the majority of the emitted power in the plane, all the interferers and target receiver are in. So, the probability to hit the receiver with the beam decreases slower than the average impact of a single hit, which leads to the greater interference. Furthermore, the less the directivity angle α the more interference is observed. The reason is that highly directional antennas concentrate the emitted power in a single beam and although only few may affect the receiver, their effect on average is higher compared to omnidirectional antennas. Enabling directivity at both Tx and Rx increases the interference even further. The effect of the density of interferers is linear when blocking is not taken into account as shown in Fig. 4(b), computed using (27), (29) and (30). The larger the value of λ_I the larger the gap between systems with directional and omnidirectional antennas. The highest interference is observed when both Tx and Rx are equipped with directions antennas.

This destructive effect of interference is mitigated by: (i) higher received signal strength compared to omnidirectional antennas, (ii) reduction in transmission power and (iii) blocking of EHF/THF radiation by the interferers themselves. The latter is a natural phenomenon of EHF/THF band that may inherently improve performance of communications.

2) The Effect of Blocking: The last two figures in Fig. 4, computed using (25), (28) and (30), show the mean interference for scenarios with omnidirectional and directional antennas, when blocking is taken into account and cone directional antenna model is used. Comparing Fig. 4(c) to Fig. 4(a), we see that the blocking drastically decreases the interference for

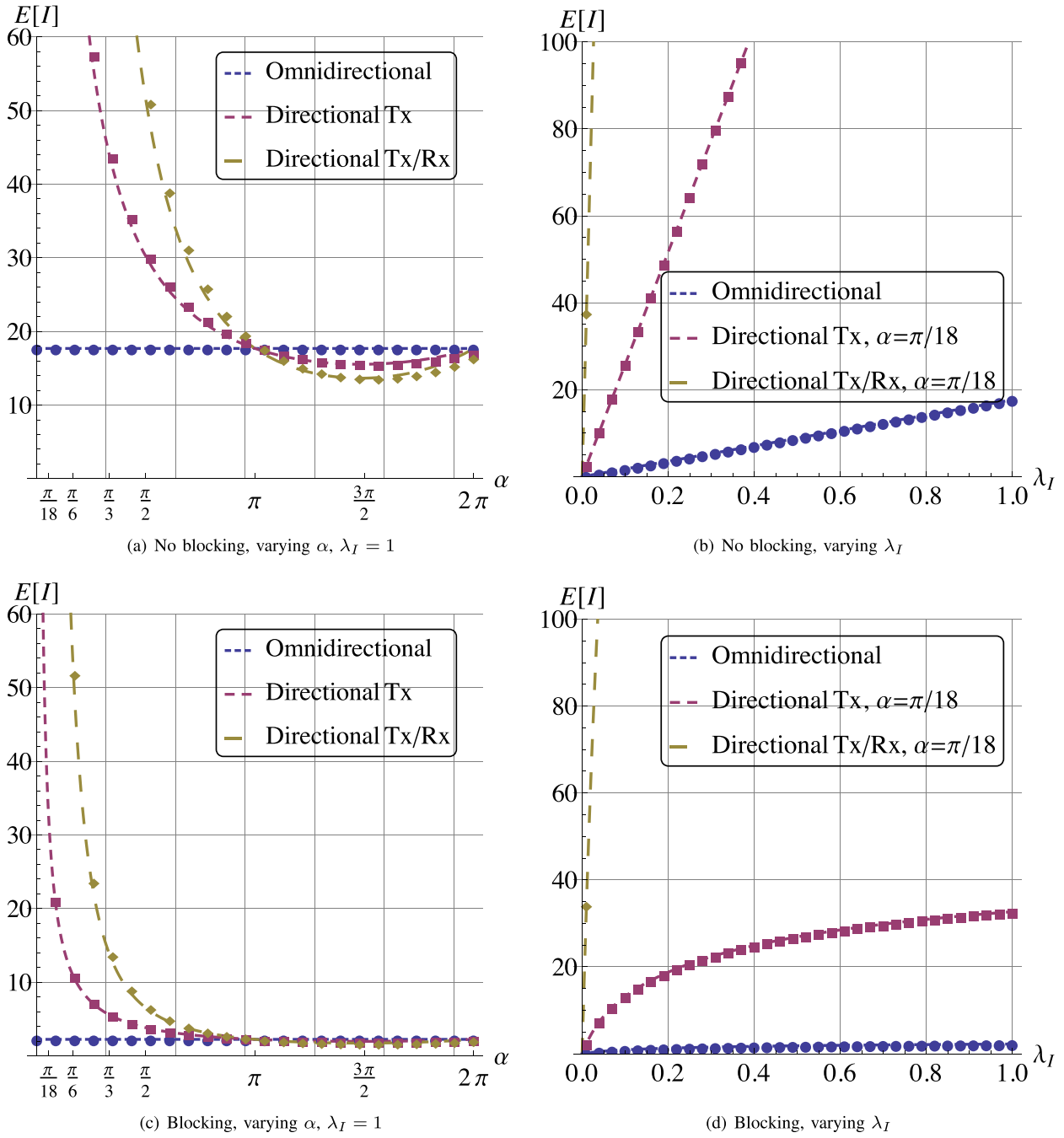

(a) No blocking, varying α, $\lambda_I = 1$

(b) No blocking, varying λ_I

(c) Blocking, varying α, $\lambda_I = 1$

(d) Blocking, varying λ_I

Fig. 4. Comparison of interference for scenarios with omnidirectional and directional cone antenna radiation pattern models.

all considered cases. Still the system with directional Tx and Rx is characterized by the highest interference.

The effect of blocking on the mean interference as a function of the interference intensity, λ_I, shown in Fig. 4(d) and computed using (25), (28) and (30), illustrates that the structure of interference principally changes when blocking is taken into account. Instead of the linear increase in response to the increase in λ_I inherent for systems without blocking, see Fig. 4(b), the increase is sublinear. Furthermore, the aggregate interference in presence of blocking does not tend to infinity as $\lambda_I \to \infty$. The reason is that, in presence of blocking, there is always a certain radius around the Rx_0 such that the interferers located outside do not contribute to the interference at Rx as their interference LoS paths are blocked.

3) The Effect of Absorption: Let us now illustrate the effect of absorption coefficient. Fig. 5, computed using (30), highlights dependence of the mean interference on the absorption coefficient K for cone directional antenna model with blocking taken into account. Fixing the density of interferers, λ_I, we observe the expected dependency on K, i.e., the interference is smaller for higher values of K, see Fig. 5(a). In general, when K increases, the interference naturally decreases due to less radiation reaching the receiver. It is important to note that this feature of EHF/THF bands is often claimed to have

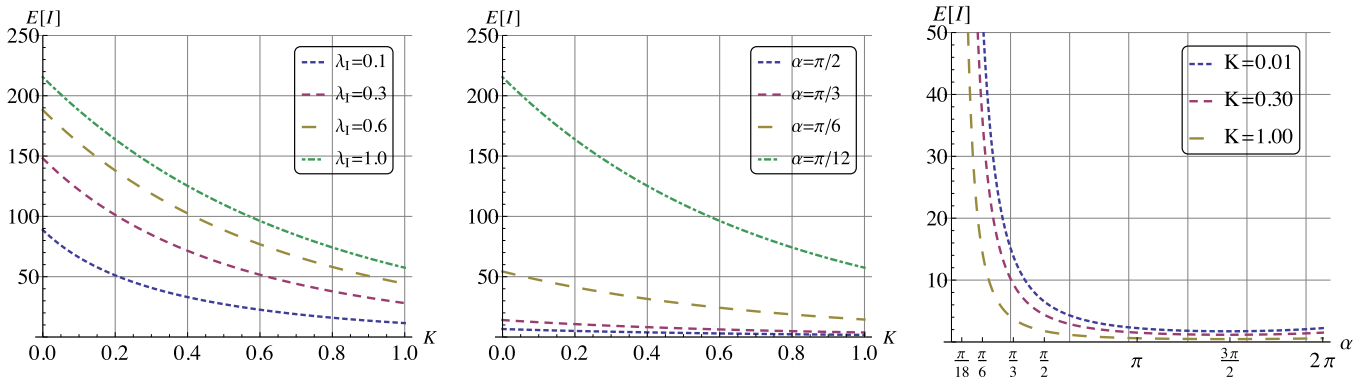

(a) Varying K, $\alpha = \pi/18$ (b) Varying K, $\lambda_I = 1$ (c) Varying α, $\lambda_I = 1$

Fig. 5. Dependence of the mean interference on the absorption coefficient K for cone directional antenna model.

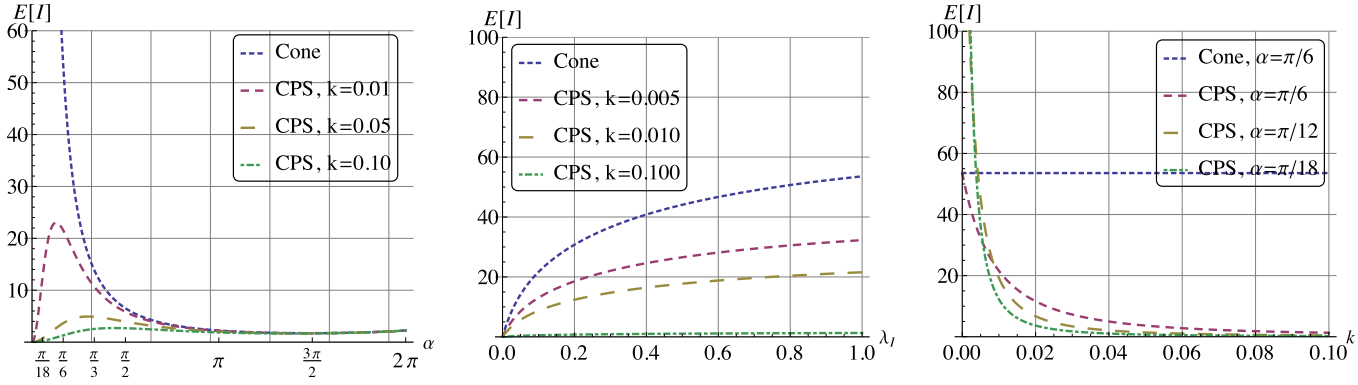

(a) Varying α, $\lambda_I = 1$ (b) Varying λ_I, $\alpha = \pi/18$ (c) Varying k, $\lambda_I = 1$

Fig. 6. Comparison of mean interference between cone and cone-plus-sphere antenna models.

negative effect. Here, we see that the proper choice of the emitted power and the operational frequency may, in fact, allow for point-to-point links creating only little interference to concurrent transmissions. Fig. 5(a) and Fig. 5(c), computed using (30), show that the effect of absorption is similar for different directivity angles.

4) The Effect of the Antenna Model: Consider the effect of different antenna radiation pattern model. Recall that according to cone model no radiation is lost to the side lobes. The cone-plus-sphere model takes into account losses to side lobes via coefficient k. The question is whether the gap between these models is large to warrant additional modeling complexity.

The mean interference as a function of the antenna directivity α for different values of loss coefficient k is shown in Fig. 6(a), computed using (30) and (34). As one may observe the behavior of the cone-plus-sphere model is more complicated compared to the cone one. When losses to side lobes are rather low, it, expectedly, resembles on the properties of the cone model. However, when k increases, the mean interference no longer tends to linear function characterizing the omnidirectional case. The dependence on λ_I is illustrated in Fig. 6(b), computed using (30) and (34). As one may observe, when losses to side lobes increases the interference decreases, i.e., the cone model greatly overestimates the actual interference. Fig. 6(c) illustrates this effect for a wide range of k and different α. Since realistic antennas are non-perfect, characterized by k in the range $0.1 \sim 0.2$ [54], no accurate approximation can be provided by the simple cone model.

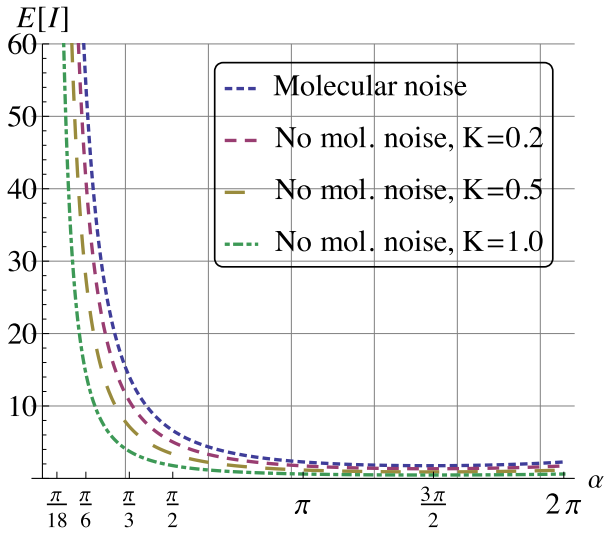

Fig. 7. Effect of molecular noise for cone antenna model.

5) The Effect of Molecular Noise: Let us analyze the effect of molecular noise. Recall that the presence of molecular

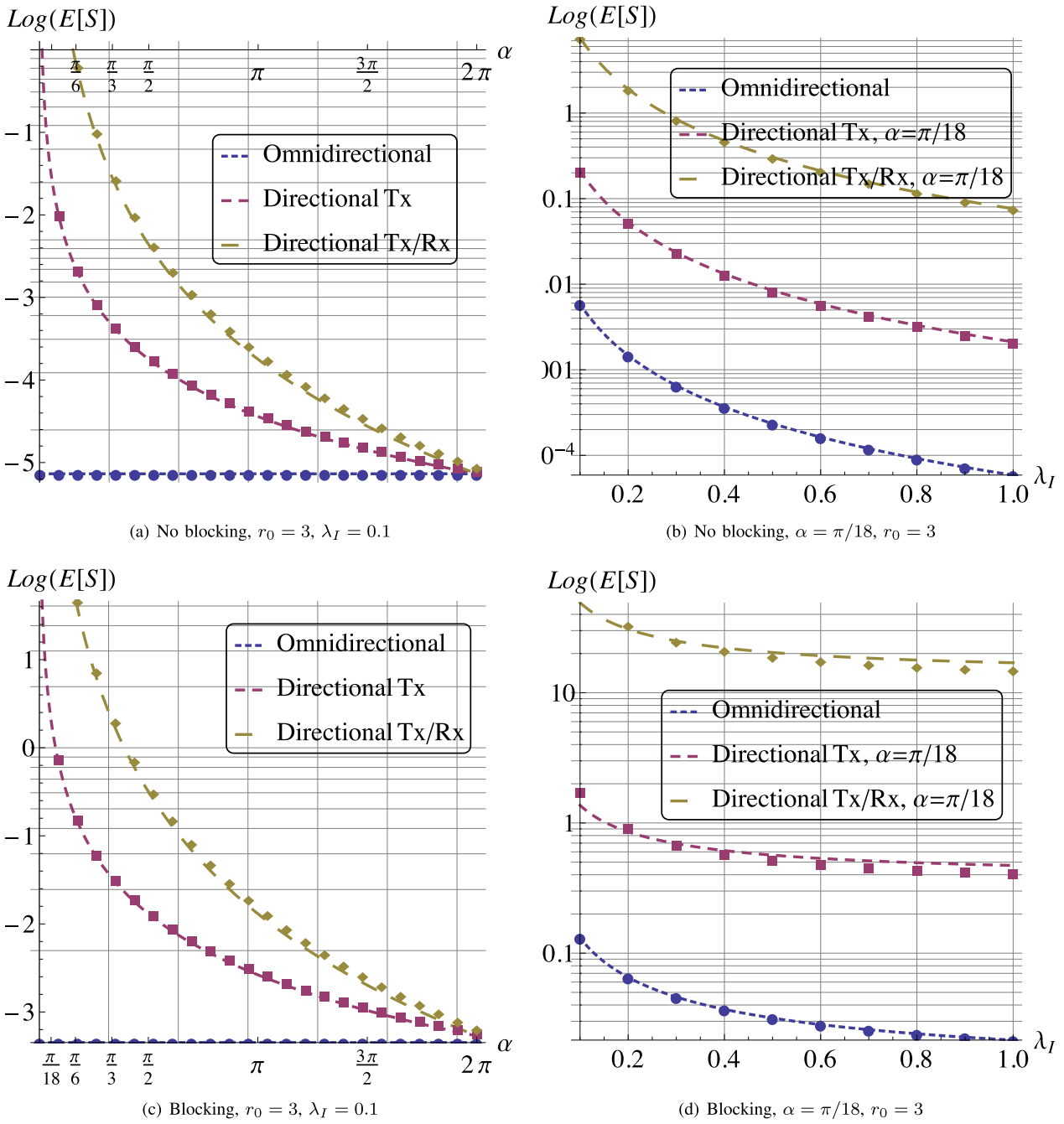

(a) No blocking, $r_0 = 3$, $\lambda_I = 0.1$

(b) No blocking, $\alpha = \pi/18$, $r_0 = 3$

(c) Blocking, $r_0 = 3$, $\lambda_I = 0.1$

(d) Blocking, $\alpha = \pi/18$, $r_0 = 3$

Fig. 8. Comparison of SINR for scenarios with omnidirectional and directional (cone) models.

noise simplifies the interference to $\sum_{i=1}^{N} A d_i^{-\gamma}$ as noise terms $(1 - e^{-Kd_i})$ now contribute to the interference at the Rx_0. Fig. 7, computed using (38), provides the comparison between scenarios where the effect of molecular noise is taken into account and neglected for cone antenna model and several values of absorption coefficient K. Expectedly, the scenario, where the molecular noise is considered leads to higher interference. When K increases from 0.2 to 0.5 to 1.0 the interference decreases.

B. SINR Assessment

The interference alone does not allow to make final conclusions about the performance of EHF/THF systems. The reason is that antenna directivity not only affects the interference but the useful received signal strength too. Below, we assess performance of the considered scenarios using mean SINR as a metric of interest concentrating on the cone antenna model.

1) The Effect of Directivity: The effect antenna directivity on the SINR, illustrated using (43) and (44), is demonstrated in Fig. 8(a) and Fig. 8(b) for $r_0 = 3$, when blocking is not taken into account. Fig. 8 also shows the results obtained by simulation of the considered scenarios. The model provides accurate SINR approximations for a wide range of input parameters. For this reason, from now on, we use the analytical model only.

As one may observe from Fig. 8(a), the system with directional antennas shows better SINR performance compared

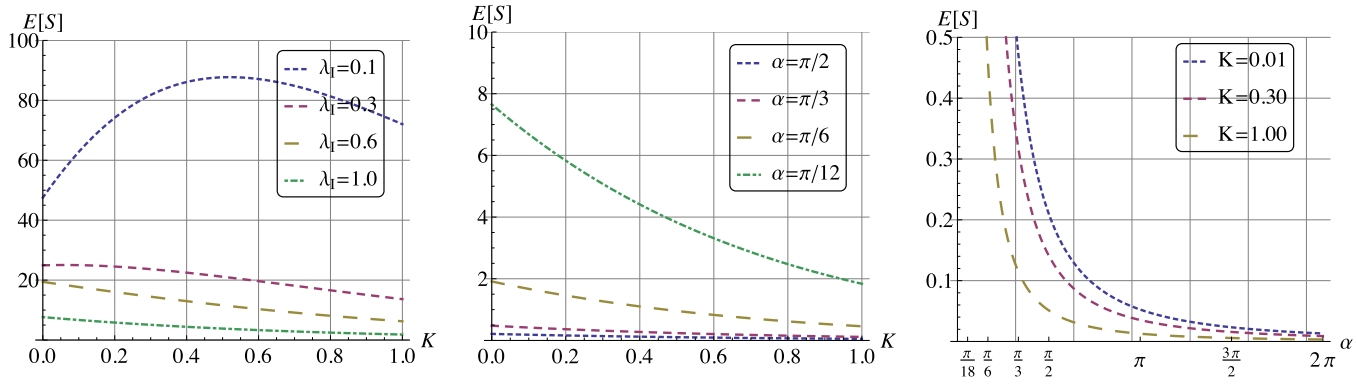

(a) Varying K, $r_0 = 3$, $\alpha = \pi/18$ (b) Varying K, $\lambda_I = \pi/18$, $r_0 = 3$ (c) Varying α, $\lambda_I = 1.0$, $r_0 = 3$

Fig. 9. Dependence of the SINR on the absorption coefficient K for cone antenna model.

to the one with omnidirectional antennas. When directivity is enabled at both sides the SINR improves even further. The SINR increases exponentially fast when the directivity of antennas increases. Recall, that the aggregated interference in this case also increases. However, it is compensated by the increase in the useful received power. We note that all the models converge to the same value for $\alpha = 2\pi$ further confirming our derivations. We also note that the substantial increase in SINR when $\alpha \to 0$ may not be achieved in real systems due to the risk of antennas misalignment between transmitter and receiver.

Fig. 8(b) highlights that the increase in the density of interferers leads to the corresponding exponential decrease of SINR. The system with directional Tx and Rx greatly outperforms the system with directional Tx or Rx while the worst performance is observed for omnidirectional antennas. The effect of the distance between Tx and Rx, r_0, on SINR has an expected behavior, that is, the SINR decreases with the increase of r_0 for all considered models, and for this reason is not shown here. The system with directional antennas at both Tx and Rx outperforms the one with omnidirectional one by approximately two orders of magnitude for all distances r_0.

2) The Effect of Blocking: Consider now the effect of blocking on SINR. Fig. 8(c), computed using (43) and (44), shows the comparison between systems when blocking is taken into account. Comparing it to the results in Fig. 8(a) for no blocking case, one may observe, that even for rather small value of interferers density, $\lambda_I = 0.1$, the blocking effect drastically increases the resulting SINR. This conclusion is valid not only for directional antennas but for omnidirectional ones as well. Note that the behavior of the mean SINR curves is qualitatively similar to those shown in Fig. 8(a). In other words, the effect of blocking affects SINR numerically only.

Fig. 8(d) shows the effect of varying interferers intensity, λ_I, on the mean SINR. Similarly to the no blocking case the mean SINR decreases as the value of λ_I increases. However, as opposed to the no blocking case, SINR does not tend to zero as $\lambda_I \to 0$. Instead, it approaches a plateau for any given antennas directivity angle α. This behavior is explained by the fact, that for any chosen values of λ_I there is always a separation distance from the Rx such that all the interferers located outside are blocked. Note that in practice, the interference from such nodes may still reach the Rx via reflections and or diffuse scattering phenomena. However, according to the recent measurements, the contributions of these components are expected to be rather weak and may not drastically change the mean SINR structure [12].

3) The Effect of Absorption Loss: The effect of absorption loss on the mean SINR for directional antennas at both Tx and Rx when blocking is taken into account is illustrated in Fig. 9, computed using (44). Observing the dependence on K in Fig. 9(a) we notice that the small values of λ_I always lead to higher SINR. However, the dependence is not linear and changes with λ_I. For small values of the intensity of interferers the mean SINR first increases approaching the maximum point and then decreases. On the other hand, for larger values of λ_I the mean SINR is a monotonously decreasing function of K. The underlying reason for this behavior is the effect of blocking and the presence of the molecular loss coefficient in both numerator and denominator of the SINR. Thus, when K and λ_I are both small, the numerator is not greatly affected by the absorption losses while blocking effectively conceal the interference in the denominator. Further, when K becomes greater than a certain value the numerator is heavily affected and the SINR decreases. For larger values of λ_I the effect of blocking cannot conceal the aggregated effect of interference even for small values of K.

Fig. 9(b), computed using (44), shows the effect of K on the mean SINR for different values of the antenna directivity angle α for directive antennas at both Tx and Rx and with blocking taken into account. Observe that for a given value of antenna directivity angle α the mean SINR decreases with the increase of K. This is explained by the effect of the denominator of the SINR. The detailed structure of the mean SINR as a function of α is further illustrated in Fig. 9(c), computed using (44). As one may observe, the mean SINR decreases as the antenna directivity increases. It is important that the gap between the environment with low and high absorption losses is high.

4) The Effect of Molecular Noise: Finally, Fig. 10 demonstrates the effect of molecular noise for a system with directional antennas at both Tx and Rx and with blocking taken into account. Recall, that according to (19), in presence of

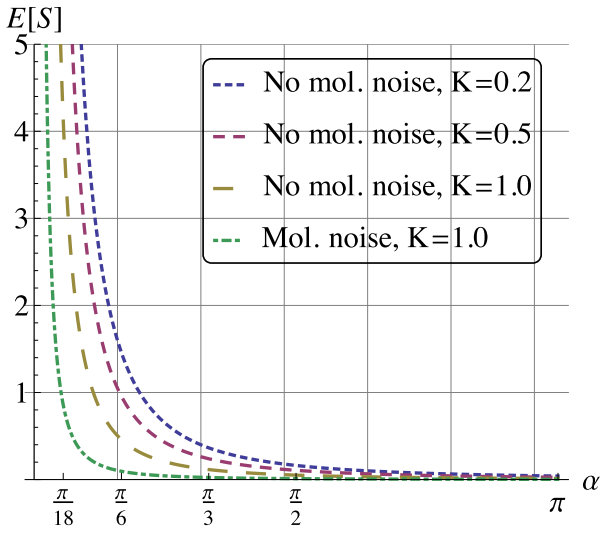

Fig. 10. Effect of molecular noise on SINR, $\lambda_I = 1$.

the molecular noise the exponential term disappears in the denominator of SINR making the aggregated interference stronger and still remains in numerator attenuating the useful received signal. Thus, expectedly, the mean SINR for $K = 1.0$ is lower compared to absence of molecular noise and $K = 1.0$ for the entire range of α. This conclusion is preserved for all intensities of interferers.

VII. Conclusions

In this paper, we have developed an analytical model for the mean interference and the SINR in mm-wave and THz communication networks. By utilizing the model, we have characterized the impact of the type of the antenna directivity and radiation pattern, the molecular absorption and blocking on aggregate interference and SINR in random Poisson deployment.

Our results show that for the same emitted power, the mean interference in a system with directional antennas drastically increases when directivity angle decreases. At the same time, the impact of the smaller directivity angle on the mean SINR is positive, as the received signal strength increases faster than the interference. The inherent property of EHF/THF bands of self-blocking of radiation by interferers leads to drastic performance improvements in terms of aggregate interference and SINR metrics compared to microwave systems. On the contrast, molecular absorption leads to the lower values of SINR. While molecular absorption loss further decreases the interference exponentially, it decreases the received signal strength too, and the effect on the latter is stronger. Finally, the effect of the molecular noise on SINR is also negative. The reason is that the useful received signal is still exponentially attenuated while the aggregated interference increases.

In our study, we have assumed that interferers completely blocks the EHF/THF radiation. In practice, reflections as well as diffuse scattering of EM waves inherent for these frequencies may still contribute to the aggregate interference at the Rx even when LoS is blocked, requiring advanced analysis.

Appendix A
Blocking Model

Here, we derive the probability of blocking using the elements of the stochastic geometry and renewal theory. The idea is to find the mean length of the blocked and open intervals at the circumference of the circle of radius x and then determine the probability of blocking of a random interferer located at x as a ratio of means of these intervals.

Consider the projection of blockers' along the radial lines as shown in Fig. 11(a). It forms a homogeneous Poisson process. Indeed, it is easy to prove that the process (i) has marginal Poisson distribution, (ii) is independent at all arc intervals, and (iii) is homogeneous. To demonstrate (i), we observe that the number of points projected at any arc of a fixed length equals to the number of points in the corresponding sector of a circle. Recalling that the number of points of a Poisson process falling into a certain area follows Poisson distribution we see that (i) holds true. The second property (ii) stems from the non-overlapping nature of sectors. Finally, (iii) is a direct consequence the homogeneity of the original Poisson process in $\Re^2$.

Let us determine the intensity of the blocker's projections on the circumference of the circle of radius x, $\lambda_P(x)$. This is accomplished by finding the mean number of points contained in the subsector of a circle defined by radii x and r_B, $S(r_B, x)$, where r_B is radius of a blocker. Recalling that the angle of the sector, α, is related to the chosen arc l_A as $\alpha = l_A/x$, while the area of the sector is related to the angle as $r^2\alpha/2$, we have

$$S(r_B, x) = \frac{l_A r_B^2}{2x}, \tag{45}$$

Expressing the area of the sector with radius x as $S(x) = l_A x/2$, the intensity $\lambda_P(x)$ is

$$\begin{aligned}\lambda_P(x) &= [S(x) - S(r_B, x)]\frac{1}{l_A}\lambda_I \\ &= \left(\frac{l_A x}{2} - \frac{l_A r_B^2}{2x}\right)\frac{\lambda_I}{l_A} = \frac{\lambda_I(x^2 - r_B^2)}{2x}.\end{aligned} \tag{46}$$

where $S(r_B, x) = l_A r_B^2/2x$ is the area of the difference between sectors of radius x and r_B, l_A is the length of the arc, r_B is the radius of the blocker.

So far we have dealt with a point process of centers of blockers. Consider now the RV W denoting the length of a "shadow'" created by an individual blocker at circumference, in Fig. 11(b). Observe that it depends on the distance from Tx to the blocker. For $r \gg 2r_B$, where r is the distance from the base of Tx to Rx, we could replace the arc ARxB by a chord AB. Since the points of the Poisson process are uniformly distributed in a circle, the probability density function (pdf) of the distance to a randomly selected blocker is

$$f_L(r; x) = \frac{2r}{x^2 - r_B^2}, \quad r_B < r < x. \tag{47}$$

Observing Fig. 11(b), by simple geometry we see that

$$W = \frac{2x r_B}{L}, \tag{48}$$

where the distance to the blocker, L, is the only RV involved.

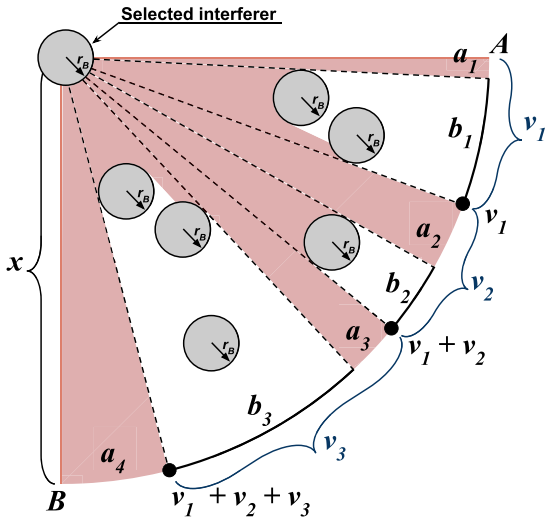

(a) The renewal process of shaded areas

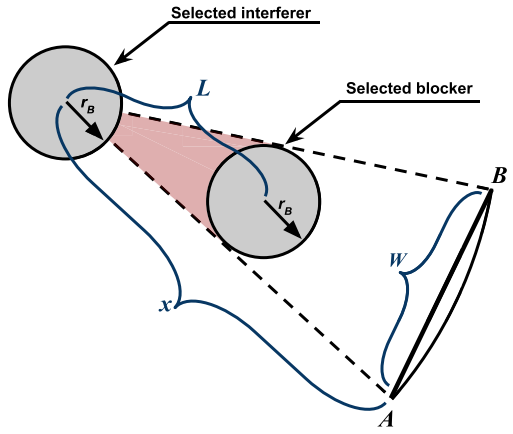

(b) The length of a blocked part

Fig. 11. Graphical illustrations of the blocking process.

The density of W can be obtained using the RV transformation technique [55]. Although the inverse function $\psi(y) = 1/x$ has a discontinuity as $x \to 0$ over the domain of L, it is continuous. The modulo of the derivative of $\psi(y)$ is $1/y^2$. Applying non-linear transformation in the form $2r_B x/L$ the pdf of W can be written as

$$f_W(y; x) = f(\psi(y))|\phi'(y)| = \frac{8x^2 r_B^2}{(x^2 - r_B^2)y^3}, \quad (49)$$

The mean of of the shadow on the circumference is then

$$E[W(x)] = \int_{2r_B}^{2x} \frac{8x^2 r_B^2}{(x^2 - r_B^2)y^3} y dy = \frac{4r_B x}{x + r_B}. \quad (50)$$

Consider now the projections of blockers onto the circumference of radius x, as shown in Fig. 11(a). The lengths of the projections of individual blockers are independent with density $f_W(x)$ and mean $E[W]$. It is easy to see that similarly to the centers of blockers, the left hand points and right hand points of individual blockers organize Poisson processes with the same intensity λ_P. The superposed process of all projections forms a renewal process with interchanging blocked and unblocked parts. An arbitrary point on the line is considered blocked if it belongs to one of the blocked interval. We find the probability of blocking as the ratio of the means of blocked interval to the sum of the means of blocked and unblocked intervals.

Let a_i b_i, $i = 1, 2, \ldots$, denote the lengths of unblocked and blocked intervals respectively, and define $v_i = a_i + b_i$. Points $0, v_1, v_1 + v_2, \ldots, \sum_{j=1}^{N} v_j, \ldots$, are the renewal moments that form the renewal process. The density of this process is [56]

$$f(x) = \lambda_P F_W(x) \exp\left(-\lambda_P \int_0^l [1 - F_W(y)]dy\right). \quad (51)$$

Let $f_V(t)$ be the pdf of v_i, $i = 1, 2, \ldots$. The functions $f_V(x)$ and $f(x)$ are related to each other via the renewal equation as [56]

$$f(x) = f_V(x) + \int_0^l f_V(x - y) f(y) dy. \quad (52)$$

The length of the unblocked part a_j follows an exponential distribution with parameter λ_P [56]. This can be verified observing that the left-hand sides of individual shadows follow Poisson process with intensity λ_P. Thus, the distance from the end of the blocked part, considered as an arbitrary point, to the starting point of the next blocked interval is exponentially distributed.

Let $F_B(x)$ and $F_V(x)$ be the CDFs of the length of blocked intervals b_i, and joint blocked/unblocked intervals, V_i, respectively, with means $E[B]$ and $E[V]$. Let further $F_B^*(s)$ and $F_V^*(s)$ be the corresponding Laplace-Stieltjes (LT) transforms. For the joint interval V_i we have

$$F_V^*(s) = F_B^*(s) F_A^*(s) = \lambda_P \frac{F_B^*(s)}{\lambda_P + s}, \quad (53)$$

which can be solved for $F_B(x)$ in the RV domain as

$$F_B(x) = F_V(x) + \frac{f_V(x)}{\lambda_P}. \quad (54)$$

When $l \to \infty$ the renewal density approaches $1/E[V]$. From (51), it also equals to $f(x) = \lambda_P \exp(-\lambda_P E[W])$. Thus,

$$E[V] = \frac{1}{\lambda_P} \exp(\lambda_P E[W]). \quad (55)$$

Consequently, $E[B]$ can now be found as

$$E[B] = \int_0^\infty \left(1 - F_V(x) - \frac{f_V(x)}{\lambda_P}\right) dx$$
$$= E[V] - \frac{1}{\mu} = \frac{1}{\lambda_P}[\exp(\lambda_P E[W]) - 1]. \quad (56)$$

The probability of blocking is thus

$$p_B(x) = \frac{E[B]}{E[A] + E[B]} = 1 - e^{-\lambda_I (x - r_B) r_B}, \quad (57)$$

where we substituted the mean of W from (50).

TABLE II
$E[I^2]$ FOR CONE ANTENNA PATTERN MODEL

Model	No molecular noise	Molecular noise
No blocking, omnidirectional	$2\pi A^2\lambda_I\Phi_1(R,r_B,K)$	$2\pi A^2\lambda_I\Phi_1^\star(R,r_B)$
Blocking, omnidirectional	$2\pi A^2\lambda_I\Phi(R,r_B,\lambda_I,K)$	$2\pi A^2\lambda_I\Phi^\star(R,r_B,\lambda_I)$
No blocking, directional Tx or Rx	$A^2\alpha\lambda_I\Phi_1(R,r_B,K)$	$A^2\alpha\lambda_I\Phi_1^\star(R,r_B)$
Blocking, directional Tx or Rx	$A^2\alpha\lambda_I\Phi(R,r_B,\lambda_I,K)$	$A^2\alpha\lambda_I\Phi^\star(R,r_B,\lambda_I)$
No blocking, directional Tx + Rx	$\frac{A^2\alpha\lambda_I}{2\pi}\Phi_1(R,r_B,K)$	$\frac{A^2\alpha\lambda_I}{2\pi}\Phi_1^\star(R,r_B)$
Blocking, directional Tx and Rx	$\frac{A^2\alpha\lambda_I}{2\pi}\Phi(R,r_B,\lambda_I,K)$	$\frac{A^2\alpha\lambda_I}{2\pi}\Phi^\star(R,r_B,\lambda_I)$

APPENDIX B
TAYLOR EXPANSION APPROXIMATION

Here, we introduce the Taylor expansion approximation, used to derive the mean SIR and SINR in Section V. Let X and Y be RVs and let $Y = g(X)$, where $y = g(x)$ is some function. According to the conventional technique, to find the pdf of Y, we need pdf of X. Also, when pdf of X is known the raw moments of Y can be found directly as

$$E[Y^v] = \int_{-\infty}^{\infty} [g(x)]^v f_X(x)dx. \tag{58}$$

In our case the pdf of interference is not known and only moments can be obtained. Thus, the task is to determine moments of Y based on the moments of X given a certain $y = g(x)$. Note that knowing the moments of SIR and SINR one may also obtain bounds in the form $Pr\{Y \le y\}$ applying Markov or Chebyshev inequalities.

Let $g(x)$ be infinitely differentiable function. Let also μ_i and β_i, $i = 0, 1, \ldots$, be the raw and central moments of X, respectively, i.e., $\mu_i = E[X^v]$, $\beta_i = E[(X-\mu_0)^v]$. Consider the Taylor series expansion of $g(x)$ around μ, that is,

$$g(x) = \sum_{i=0}^{\infty} \frac{g^{(i)}(\mu_0)}{i!}(x-\mu_0)^i. \tag{59}$$

Taking expectations from both sides of (59) we get

$$E[g(x)] = \sum_{i=0}^{\infty} \frac{g^{(i)}(\mu_0)}{i!}E[(x-\mu_0)^i]. \tag{60}$$

where $g^{(i)}(x)$ denotes ith derivative of $g(x)$.

Noting that $\beta_i = E[(x-\mu_0)^i]$, $E[g(x)] = E[Y]$ we it as

$$E[Y] = \sum_{i=0}^{\infty} \frac{g^{(i)}(\mu_0)}{i!}\beta_i. \tag{61}$$

Knowing the central moments of X and leaving a certain amount of terms in (61) we could approximate the mean of Y with any given accuracy. For practical applications two or three terms often suffice. Analyzing (61) one may observe that the first term $\beta_1 = E[X-\mu_0]$ is always zero. Thus, in what follows, we use

$$E[Y] = g(\mu_0) + \frac{g''(\mu_0)}{2}\sigma^2[X], \tag{62}$$

where $\sigma^2[X]$ is the variance of X.

Let $a_i = g^{(i)}/i!$ and consider the variance of Y. Using $\sigma^2[Y] = E[Y^2] - (E[Y])^2$ we can show

$$\begin{aligned}(E[Y])^2 &= \sum_{i=0}^{\infty} a_i^2\beta_i^2 + \sum_{i=0}^{\infty} a_i\beta_i \sum_{j=i+1}^{\infty} a_j\beta_j \\ &= a_0^2 + 2a_0\sum_{i=2}^{\infty} a_i\beta_i + \left(\sum_{i=2}^{\infty} a_i\beta_i\right)^2,\end{aligned} \tag{63}$$

where we separated quadratic and linear terms.

Using the Taylor series expansion around μ, squaring it and taking expectations we arrive at

$$E[Y^2] = \sum_{i=0}^{\infty} b_i\beta_i, \tag{64}$$

where the sequence b_i is given by

$$b_i = \begin{cases} a_{i/2}^2 + 2\sum_{k=0}^{i/2-1} a_k a_{i-k}, & i \text{ is even} \\ 2\sum_{k=0}^{\lfloor n/2\rfloor} a_k a_{i-k}, & i \text{ is odd,} \end{cases} \tag{65}$$

and $\lfloor\cdot\rfloor$ denotes the floor function.

Leaving linear terms in (63) and (64) and simplifying

$$\sigma^2[Y] = \sum_{i=2}^{\infty} c_i\beta_i + \left(\sum_{i=2}^{\infty} a_i\beta_i\right)^2, \tag{66}$$

where the sequence c_i is

$$c_i = \begin{cases} a_{i/2}^2 + 2\sum_{k=1}^{i/2-1} a_k a_{i-k}, & i \text{ is even} \\ 2\sum_{k=1}^{\lfloor n/2\rfloor} a_k a_{i-k}, & i \text{ is odd.} \end{cases} \tag{67}$$

The approximation for variance is now given by

$$\sigma^2[Y] = [g'(\mu_0)]^2\sigma^2[X] - \frac{1}{4}[f''(\mu_0)\sigma^2[X]]^2, \tag{68}$$

where we also included the qudratic correction term.

APPENDIX C
VARIANCE OF INTERFERENCE

There are two ways to find variance of interference. According to the first approach we (i) determine the distribution of distance to a randomly chosen interferer that is not blocked,

$$\Phi = \frac{4R^2(K+\lambda_I r_B)^2 e^{2R(K+\lambda_I r_B)} Ei(2R(r_B\lambda_I+K)) + 2KR + 2\lambda_I R r_B - 1}{2R^2 e^{-2\lambda_I r_B(r_B-R)-2KR}}\Bigg|_{r_B}^{R} \tag{70}$$

$$\Phi_1(R, r_B, K) = \left(2K^2 Ei(-2KR) + e^{-2KR}\left(\frac{K}{R} - \frac{1}{2R^2}\right)\right)\Bigg|_{r_B}^{R},$$

$$\Phi_1^{\star}(R, r_B) = \frac{1}{2r_B^2} - \frac{1}{2R^2}, \quad \Phi^{\star}(R, r_B, \lambda_I) = \frac{\lambda_I^2 R^2 r_B^2 e^{\lambda_I R r_B} Ei(-Rr_B\lambda_I) + \lambda_I R r_B - 1}{2R^2 e^{-\lambda_I r_B(r_B-R)}}\Bigg|_{r_B}^{R} \tag{71}$$

(ii) estimate the moments of the interference from this nodes, (iii) observe that the number of non-blocked interferers follows Poisson distribution with reduced intensity and, finally, (iv) obtain the variance of aggregated interference as a variance of a random sum of RVs, see, e.g., [55]. Note that this approach can also be used to find mean interference (via Wild's identity) and it is feasible due to finite mean and variance of interference from a single node.

In what follows, we rely on the approach similar to that we used for finding mean interference in Sec. IV. Particularly, representing the variance of interference as $\sigma^2[I] = E[I^2] - (E[I])^2$ we will be looking for $E[I^2]$. Owing to the independence of the RVs representing the number of points of a Poisson process in non-overlapping areas we use integral expressions to get $E[I^2]$. Since the derivation is similar for all considered cases, we demonstrate the approach it for cone antenna model with blocking and Tx (or Rx) directivity.

Taking into account Tx (or Rx) directivity and blocking we write

$$E[I^2] = \int_{r_B}^{R} \left(Ar^{-2}e^{-Kr}\right)^2 e^{-\lambda_I(x-r_B)r_B} \frac{\alpha}{2\pi} 2\lambda_I \pi r dr$$
$$= \frac{A^2\alpha^2\lambda_I}{2\pi}\Phi(R, r_B, \lambda_I, K), \tag{69}$$

where $\Phi(R, r_B, \lambda_I, K)$ is given in (70), as shown at the top of this page. The second raw moment for cone antenna model without blocking and/or directivity is found similarly to (69). Also, one can use this approach to obtain $E[I^2]$ for cone-plus-sphere model. The resulting expressions for cone antenna models are shown in Table II, where $\Phi_1(R, r_B, K)$, $\Phi_1^{\star}(R, r_B)$, and $\Phi^{\star}(R, r_B, \lambda_I)$ are given in (71), as shown at the top of this page.

REFERENCES

[1] V. Petrov, M. Komarov, D. Moltchanov, J. M. Jornet, and Y. Koucheryavy, "Interference analysis of EHF/THF communications systems with blocking and directional antennas," in *Proc. IEEE Global Commun. Conf. (GLOBECOM)*, Dec. 2016, pp. 1–7.

[2] *Cisco Visual Networking Index: Global Mobile Data Traffic Forecast Update 2014–2019*, Cisco, San Jose, CA, USA, 2015.

[3] "The 1000x mobile data challenge," Qualcomm, San Diego, CA, USA, Tech. Rep., 2013. [Online]. Available: HTTPS://www.qualcomm.com/media/documents/files/1000x-mobile-datachallenge. pdf

[4] Y. Niu, Y. Li, D. Jin, L. Su, and A. V. Vasilakos, "A survey of millimeter wave communications (mmWave) for 5G: Opportunities and challenges," *Wireless Netw.*, vol. 21, no. 8, pp. 2657–2676, Nov. 2015.

[5] S. Rey, *TERAPAN: Ultra-high Data Rate Transmission With Steerable Antennas at 300 GHz*, IEEE Standard 802.15-15-0167-02-0thz, Mar. 2015.

[6] J. Boyd. (Oct. 2015). *Fujitsu Makes a Terahertz Receiver Small Enough for a Smartphone*. [Online]. Available: http://www.spectrum.ieee.org/tech-talk/telecom/wireless/fujitsu-makes-a-terahertz-receiver-small-enough-for-a-smartphone

[7] V. Petrov, D. Moltchanov, and Y. Koucheryavy, "Applicability assessment of terahertz information showers for next-generation wireless networks," in *Proc. IEEE Int. Conf. Commun. (ICC)*, May 2016, pp. 1–7.

[8] I. Akyildiz, J. Jornet, and C. Han, "TeraNets: Ultra-broadband communication networks in the terahertz band," *IEEE Wireless Commun. Mag.*, vol. 21, no. 4, pp. 130–135, Aug. 2014.

[9] S. Kim, W. T. Khan, A. Zajić, and J. Papapolymerou, "D-band channel measurements and characterization for indoor applications," *IEEE Trans. Antennas Propag.*, vol. 63, no. 7, pp. 3198–3207, Jul. 2015.

[10] V. Petrov, A. Pyattaev, D. Moltchanov, and Y. Koucheryavy, "Terahertz band communications: Applications, research challenges, and standardization activities," in *Proc. Int. Cong. Ultra Modern Telecommun. Control Syst. (ICUMT)*, Oct. 2016, pp. 183–190.

[11] S. Kim and A. G. Zajić, "Statistical characterization of 300-GHz propagation on a desktop," *IEEE Trans. Veh. Technol.*, vol. 64, no. 8, pp. 3330–3338, Aug. 2015.

[12] M. R. Akdeniz *et al.*, "Millimeter wave channel modeling and cellular capacity evaluation," *IEEE J. Sel. Areas Commun.*, vol. 32, no. 6, pp. 1164–1179, Jun. 2014.

[13] J. M. Jornet and I. F. Akyildiz, "Channel modeling and capacity analysis for electromagnetic wireless nanonetworks in the terahertz band," *IEEE Trans. Wireless Commun.*, vol. 10, no. 10, pp. 3211–3221, Oct. 2011.

[14] L. S. Rothman *et al.* (2014). *HITRAN: High-Resolution Transmission Molecular Absorption Database Harvard-Smithson Center for Astrophysics*. [Online]. Available: https://www.cfa.harvard.edu

[15] J. G. Andrews *et al.*, "What will 5G be?" *IEEE J. Sel. Areas Commun.*, vol. 32, no. 6, pp. 1065–1082, Jun. 2014.

[16] N. Bhushan *et al.*, "Network densification: The dominant theme for wireless evolution into 5G," *IEEE Commun. Mag.*, vol. 52, no. 2, pp. 82–89, Feb. 2014.

[17] J. G. Andrews, H. Claussen, M. Dohler, S. Rangan, and M. C. Reed, "Femtocells: Past, present, and future," *IEEE J. Sel. Areas Commun.*, vol. 30, no. 3, pp. 497–508, Apr. 2012.

[18] J. Lee, H. Wang, J. G. Andrews, and D. Hong, "Outage probability of cognitive relay networks with interference constraints," *IEEE Trans. Wireless Commun.*, vol. 10, no. 2, pp. 390–395, Feb. 2011.

[19] G. Fodor, S. Parkvall, S. Sorrentino, P. Wallentin, Q. Lu, and N. Brahmi, "Device-to-device communications for national security and public safety," *IEEE Access*, vol. 2, pp. 1510–1520, Dec. 2014.

[20] T. Bai, R. Vaze, and R. W. Heath, Jr., "Using random shape theory to model blockage in random cellular networks," in *Proc. Int. Conf. Signal Process. Commun. (SPCOM)*, Jul. 2012, pp. 1–5.

[21] T. Bai, R. Vaze, and R. W. Heath, Jr., "Analysis of blockage effects on urban cellular networks," *IEEE Trans. Wireless Commun.*, vol. 13, no. 9, pp. 5070–5083, Sep. 2014.

[22] J. Kokkoniemi, V. Petrov, D. Moltchanov, J. Lehtomaki, Y. Koucheryavy, and M. Juntti, "Wideband terahertz band reflection and diffuse scattering measurements for beyond 5G indoor wireless networks," in *Proc. Eur. Wireless Conf.*, May 2016, pp. 1–6.

[23] S. Kim and A. Zajić, "Statistical modeling and simulation of short-range device-to-device communication channels at sub-THz frequencies," *IEEE Trans. Wireless Commun.*, vol. 15, no. 9, pp. 6423–6433, Sep. 2016.

[24] M. Gapeyenko *et al.*, "Analysis of human body blockage in millimeter-wave wireless communications systems," in *Proc. IEEE Int. Conf. Commun. (ICC)*, May 2016, pp. 1–7.

[25] J. G. Andrews, R. K. Ganti, M. Haenggi, N. Jindal, and S. Weber, "A primer on spatial modeling and analysis in wireless networks," *IEEE Commun. Mag.*, vol. 48, no. 11, pp. 156–163, Nov. 2010.

[26] P. Cardieri, "Modeling interference in wireless ad hoc networks," *IEEE Commun. Surveys Tuts.*, vol. 12, no. 4, pp. 551–572, 4th Quart., 2010.

[27] M. Z. Win, P. C. Pinto, and L. A. Shepp, "A mathematical theory of network interference and its applications," *Proc. IEEE*, vol. 97, no. 2, pp. 205–230, Feb. 2009.
[28] M. Haenggi, J. G. Andrews, F. Baccelli, O. Dousse, and M. Franceschetti, "Stochastic geometry and random graphs for the analysis and design of wireless networks," *IEEE J. Sel. Areas Commun.*, vol. 27, no. 7, pp. 1029–1046, Sep. 2009.
[29] M. Haenggi, "Mean interference in hard-core wireless networks," *IEEE Commun. Lett.*, vol. 15, no. 8, pp. 792–794, Aug. 2011.
[30] H. ElSawy and E. Hossain, "On stochastic geometry modeling of cellular uplink transmission with truncated channel inversion power control," *IEEE Trans. Wireless Commun.*, vol. 13, no. 8, pp. 4454–4469, Aug. 2014.
[31] A. K. Gupta, X. Zhang, and J. G. Andrews, "SINR and throughput scaling in ultradense urban cellular networks," *IEEE Wireless Commun. Lett.*, vol. 4, no. 6, pp. 605–608, Dec. 2015.
[32] K. Venugopal and R. W. Heath, Jr., "Millimeter wave networked wearables in dense indoor environments," *IEEE Access*, vol. 4, pp. 1205–1221, Mar. 2016.
[33] A. Thornburg, T. Bai, and R. W. Heath, Jr., "Interference statistics in a random mmwave ad hoc network," in *Proc. IEEE Int. Conf. Acoust., Speech Signal Process. (ICASSP)*, Apr. 2015, pp. 2904–2908.
[34] K. Venugopal and R. W. Heath, Jr., "Location based performance model for indoor mmWave wearable communication," in *Proc. IEEE Int. Conf. Commun. (ICC)*, May 2016, pp. 1–6.
[35] K. Venugopal, M. C. Valenti, and R. W. Heath, Jr., "Interference in finite-sized highly dense millimeter wave networks," in *Proc. Inf. Theory Appl. Workshop (ITA)*, Feb. 2015, pp. 175–180.
[36] M. Di Renzo, "Stochastic geometry modeling and analysis of multi-tier millimeter wave cellular networks," *IEEE Trans. Wireless Commun.*, vol. 14, no. 9, pp. 5038–5057, Sep. 2015.
[37] S. Singh, M. N. Kulkarni, A. Ghosh, and J. G. Andrews, "Tractable model for rate in self-backhauled millimeter wave cellular networks," *IEEE J. Sel. Areas Commun.*, vol. 33, no. 10, pp. 2196–2211, Oct. 2015.
[38] M. Rebato, M. Mezzavilla, S. Rangan, F. Boccardi, and M. Zorzi. (Apr. 2016). "Understanding noise and interference regimes in 5G millimeter-wave cellular networks." [Online]. Available: https://arxiv.org/abs/1604.05622
[39] M. Rebato, "Simulation analysis of algorithms for interference management in 5G cellular networks using spatial spectrum sharing," Ph.D. dissertation, Dept. Inf. Eng., Univ. Padua, Italy, Italy, 2015.
[40] J. M. Jornet and I. F. Akyildiz, "Low-weight channel coding for interference mitigation in electromagnetic nanonetworks in the terahertz band," in *Proc. IEEE Int. Conf. Commun. (ICC)*, Jun. 2011, pp. 1–6.
[41] V. Petrov, D. Moltchanov, and Y. Koucheryavy, "Interference and SINR in dense terahertz networks," in *Proc. IEEE Veh. Technol. Conf. (VTC-Fall)*, Sep. 2015, pp. 1–5.
[42] S. Singh, R. Mudumbai, and U. Madhow, "Interference analysis for highly directional 60-GHz mesh networks: The case for rethinking medium access control," *IEEE/ACM Trans. Netw.*, vol. 19, no. 5, pp. 1513–1527, Oct. 2011.
[43] L. X. Cai, L. Cai, X. Shen, and J. W. Mark, "REX: A randomized exclusive region based scheduling scheme for mmWave WPANs with directional antenna," *IEEE Trans. Wireless Commun.*, vol. 9, no. 1, pp. 113–121, Jan. 2010.
[44] M. X. Gong, R. Stacey, D. Akhmetov, and S. Mao, "A directional CSMA/CA protocol for mmWave wireless PANs," in *Proc. IEEE Wireless Commun. Netw. Conf. (WCNC)*, Apr. 2010, pp. 1–6.
[45] E. Shihab, L. Cai, and J. Pan, "A distributed asynchronous directional-to-directional MAC protocol for wireless ad hoc networks," *IEEE Trans. Veh. Technol.*, vol. 58, no. 9, pp. 5124–5134, Nov. 2009.
[46] Q. Xia, Z. Hossain, M. Medley, and J. M. Jornet, "A link-layer synchronization and medium access control protocol for terahertz-band communication networks," in *Proc. IEEE Global Commun. Conf. (GLOBECOM)*, Dec. 2015, pp. 1–7.
[47] J. M. Jornet and I. F. Akyldiz, "Femtosecond-long pulse-based modulation for terahertz band communication in nanonetworks," *IEEE Trans. Commun.*, vol. 62, no. 5, pp. 1742–1754, May 2014.
[48] S. Chandrasekhar, *Radiative Transfer*. New York, NY, USA: Dover, 1960.
[49] P. Boronin, V. Petrov, D. Moltchanov, Y. Koucheryavy, and J. M. Jornet, "Capacity and throughput analysis of nanoscale machine communication through transparency windows in the terahertz band," *Nano Commun. Netw.*, vol. 5, no. 3, pp. 72–82, Sep. 2014.
[50] J. Kokkoniemi, J. Lehtomäki, and M. Juntti, "A discussion on molecular absorption noise in the terahertz band," *Nano Commun. Netw.*, vol. 8, pp. 35–45, Jun. 2016.
[51] L. B. Kish, "Stealth communication: Zero-power classical communication, zero-quantum quantum communication and environmental-noise communication," *Appl. Phys. Lett.*, vol. 87, no. 23, p. 234109, Dec. 2005.
[52] N. Atindra and A. Ghosh, "Ultralow noise field-effect transistor from multilayer graphene," *Appl. Phys. Lett.*, vol. 95, no. 8, p. 082105, Aug. 2009.
[53] V. Petrov, D. Moltchanov, and Y. Koucheryavy, "On the efficiency of spatial channel reuse in ultra-dense THz networks," in *Proc. IEEE Global Commun. Conf. (GLOBECOM)*, Dec. 2015, pp. 1–7.
[54] T. S. Rappaport, *Wireless Communications: Principles Practice*. Englewood Cliffs, NJ, USA: Prentice-Hall, 2002.
[55] S. Ross, *Introduction to Probability Models*. San Francisco, CA, USA: Academic, 2010.
[56] D. R. Cox, *Renewal Theory*. London, U.K.: Methuen, 1970.

Vitaly Petrov (S'15) received the M.Sc. degree in information systems security from the Saint Petersburg State University of Aerospace Instrumentation, Saint Petersburg, Russia, in 2011, and the M.Sc. degree in communications engineering from the Tampere University of Technology, Tampere, Finland, in 2014, where he is currently pursuing the Ph.D. degree, where he is involved in enabling terahertz band communications for beyond 5G wireless networks. He was a Visiting Scholar with the Georgia Institute of Technology, Atlanta, USA, in 2014, and a Strategic Intern with the Nokia Research Center, Helsinki, Finland, in 2012. His current research interests include the Internet-of-Things, terahertz band communications, nanonetworks, cryptology, and network security.

Mikhail Komarov (M'14) received the M.Sc. and Cand.Sc. degrees from the Moscow State Institute of Electronics and Mathematics (Technical University), in 2010 and 2012, respectively. He is currently pursuing the Ph.D. degree with the Department of Electronics and Communications Engineering, Tampere University of Technology, Finland. He has authored over 30 publications. His research interests include the energy efficiency of wireless sensor networks, heterogeneous networks and network challenges with the connection to big data area, e-business and e-commerce, social web of things, Internet of Things, and mobile applications networks.

Dmitri Moltchanov received the M.Sc. and Cand.Sc. degrees from the St. Petersburg State University of Telecommunications, Russia, in 2000 and 2002, respectively, and the Ph.D. degree from the Tampere University of Technology in 2006. He is a Senior Research Scientist with the Department of Electronics and Communications Engineering, Tampere University of Technology, Finland. He has authored over 100 publications. His research interests include performance evaluation and optimization issues of wired and wireless IP networks, Internet traffic dynamics, quality of user experience of real-time applications, and mmWave/terahertz communications systems. He serves as a TPC member in a number of international conferences.

Josep Miquel Jornet (M'13) received the B.S. degree in telecommunication engineering and the M.Sc. degree in information and communication technologies from the Universitat Politècnica de Catalunya, Barcelona, Spain, in 2008, and the Ph.D. degree in electrical and computer engineering from the Georgia Institute of Technology (Georgia Tech), Atlanta, GA, USA, in 2013. He received a Fellowship from "la Caixa" (2009–2010) and Fundación Caja Madrid (2011–2012). From 2007 to 2008, he was a Visiting Researcher with the Massachusetts Institute of Technology (MIT), Cambridge, MA, USA, under the MIT Sea Grant Program. He is currently an Assistant Professor with the Department of Electrical Engineering, University at Buffalo, The State University of New York, Buffalo, NY, USA. His current research interests include terahertz-band communication networks, nano-photonic wireless communication, graphene-enabled wireless communications, intra-body wireless nanosensor networks, and the Internet of Nano-Things. He is a member of the ACM. He was the recipient of the Oscar P. Cleaver Award for outstanding graduate students in the School of Electrical and Computer Engineering, Georgia Tech, in 2009. He also received the Broadband Wireless Networking Lab Researcher of the Year Award in 2010. In 2016, he received the Distinguished TPC Member Award at the IEEE International Conference on Computer Communications (INFOCOM) 2016, one of the premier conferences of the IEEE Communications Society. Since 2016, he has been an Editor-in-Chief of the *Nano Communication Networks (Elsevier) Journal*.

Yevgeni Koucheryavy (SM'09) received the Ph.D. degree from the Tampere University of Technology (TUT), Finland. He is currently a Professor and Lab Director with the Department of Electronics and Communications Engineering, TUT. He is the author of numerous publications in the field of advanced wired and wireless networking and communications. His current research interests include various aspects in heterogeneous wireless communication networks and systems, the Internet of Things and its standardization, and nanocommunications. He is Associate Technical Editor of the *IEEE Communications Magazine* and an Editor of the IEEE COMMUNICATIONS SURVEYS AND TUTORIALS.